Earth and Planetary Science Letters 317-318 (2012) 27–43

Contents lists available at SciVerse ScienceDirect

Earth and Planetary Science Letters

journal homepage: www.elsevier.com/locate/epsl

A geophysical perspective on mantle water content and melting: Inverting electromagnetic sounding data using laboratory-based electrical conductivity profiles

A. Khan [a,*], T.J. Shankland [b]

[a] Institute of Geochemistry and Petrology, Swiss Federal Institute of Technology, Zürich, Switzerland
[b] Geophysics Group, Los Alamos National Laboratory, Los Alamos, USA

ARTICLE INFO

Article history:
Received 21 July 2011
Received in revised form 29 October 2011
Accepted 19 November 2011
Available online 27 December 2011

Editor: L. Stixrude

Keywords:
mantle composition
thermal state
electrical conductivity
water content
electromagnetic sounding
inverse problems

ABSTRACT

This paper applies electromagnetic sounding methods for Earth's mantle to constrain its thermal state, chemical composition, and "water" content. We consider long-period inductive response functions in the form of *C*-responses from four stations distributed across the Earth (Europe, North America, Asia and Australia) covering a period range from 3.9 to 95.2 days and sensitivity to ~1200 km depth. We invert *C*-responses directly for thermo-chemical state using a self-consistent thermodynamic method that computes phase equilibria as functions of pressure, temperature, and composition (in the Na_2O–CaO–FeO–MgO–Al_2O_3–SiO_2 model system). Computed mineral modes are combined with recent laboratory-based electrical conductivity models from independent experimental research groups (Yoshino (2010) and Karato (2011)) to compute bulk conductivity structure beneath each of the four stations from which *C*-responses are estimated. To reliably allocate water between the various mineral phases we include laboratory-measured water partition coefficients for major upper mantle and transition zone minerals. This scheme is interfaced with a sampling-based algorithm to solve the resulting non-linear inverse problem. This approach has two advantages: (1) It anchors temperatures, composition, electrical conductivities, and discontinuities that are in laboratory-based forward models, and (2) At the same time it permits the use of geophysical inverse methods to optimize conductivity profiles to match geophysical data. The results show lateral variations in upper mantle temperatures beneath the four stations that appear to persist throughout the upper mantle and parts of the transition zone. Calculated mantle temperatures at 410 and 660 km depth lie in the range 1250–1650 °C and 1500–1750 °C, respectively, and generally agree with the experimentally-determined temperatures at which the measured phase reactions olivine → β-spinel and γ-spinel → ferropericlase + perovskite occur. The retrieved conductivity structures beneath the various stations tend to follow trends observed for temperature with the strongest lateral variations in the uppermost mantle; for depths > 300 km conductivities appear to depend less on the particular conductivity database. Conductivities at 410 km and at 660 km depth are found to agree overall with purely geophysically-derived global and semi-global one-dimensional conductivity models. Both electrical conductivity databases point to <0.01 wt.% H_2O in the upper mantle. For transition zone minerals results from the laboratory database of Yoshino (2010) suggest that a much higher water content (up to 2 wt.% H_2O) is required than in the other database (Karato, 2011), which favors a relatively "dry" transition zone (<0.01 wt.% H_2O). Incorporating laboratory measurements of hydrous silicate melting relations and available conductivity data allows us to consider the possibility of hydration melting and a high-conductivity melt layer above the 410-km discontinuity. The latter appears to be 1) regionally localized and 2) principally a feature from the Yoshino (2010) database. Further, there is evidence of lateral heterogeneity: The mantle beneath southwestern North America and central China appears "wetter" than that beneath central Europe or Australia.

© 2011 Elsevier B.V. All rights reserved.

1. Introduction

Water has and continues to play an important role in determining the evolution of Earth through its influence on such critical processes as chemical differentiation and geodynamical evolution. This results from the strong influence of water on dynamical behavior of the mantle, including its creep strength, melting relations, phase transitions, transport, and physical rock properties (e.g. Hirth and Kohlstedt, 1996; Hofmeister, 2004; Karato, 1990, 2006; Karato and Jung, 2003; Litasov and Ohtani, 2007; Mao et al., 2008; Mei and Kohlstedt, 2000; Peslier et al., 2010; Smyth and Frost, 2002; Wood, 1995).

The total water inventory of the Earth is not well-constrained with values ranging from the equivalent of half an ocean to as much as 5 or

* Corresponding author.
E-mail address: amir.khan@erdw.ethz.ch (A. Khan).

0012-821X/$ – see front matter © 2011 Elsevier B.V. All rights reserved.
doi:10.1016/j.epsl.2011.11.031

more oceans (e.g., Ahrens, 1989; Hirschmann et al., 2005; Ringwood, 1975). However, much experimental work has been conducted since Smyth (1987) suggested that wadsleyite, a major transition zone mineral, can incorporate significant amounts of water in its crystal structure, implying that the mantle could store the equivalent of several oceans of water. This, however, is not the only possible mode for storing water in the mantle. Hydrous fluids and melts that are related to melting processes occurring at a number of locations in the mantle present other means. These are likely to be found in mantle wedges above subduction zones, within mid-ocean ridge basalt (MORB) and ocean-island basalt (OIB) source regions, and in up- and downwellings across the transition zone (e.g. Hirschmann, 2006). Moreover, such hydrous fluid or melt layers, even on a localized scale, may act to critically modulate the flux of water and chemical elements between the upper mantle, transition zone (TZ) and lower mantle (e.g., Bercovici and Karato, 2003; Ohtani et al., 2004). However, the exact amount, location and mechanism of exchange of water between various mantle reservoirs are yet to be fully understood (e.g. Hirschmann et al., 2005; Keppler and Bolfan-Casanova, 2006). Improving the understanding of deep water cycles and their relations to mantle dynamics thus hinges crucially on characterizing these reservoirs as accurately as possible.

Current estimates of mantle water content rely mostly on sample analyses of MORB and OIB material, mantle xenoliths, as well as on cosmochemical and geochemical arguments. MORB and OIB sources imply an upper mantle containing between 0.0005–0.02 and 0.03–0.1 wt.% H_2O, respectively, while bulk silicate Earth is geochemically constrained to contain between 0.05 and 0.19 wt.% H_2O (see e.g. Bolfan-Casanova et al., 2006; Hirschmann, 2006; Keppler and Bolfan-Casanova, 2006 for recent reviews). Of prime interest in the context of these estimates is the concept of water storage capacity, which is the maximum amount of water that a mineral or rock at a given pressure and temperature is able to retain without producing a hydrous fluid (water- or silicate-rich). The importance of storage capacity arises because different minerals have different storage capacities, which in turn limits potential reservoirs. Much recent work has thus focused on assessing the compatibility of the above estimates with constraints on H_2O storage capacity of different minerals as a function of depth derived from experimental petrology and mineral physics. Briefly, storage capacity of the upper mantle at 400 km depth is likely to be between 0.05 and 0.5 wt.% H_2O (Hirschmann et al., 2005, 2009) based on measurements performed on major upper mantle minerals olivine, orthopyroxene and garnet (e.g., Aubaud et al., 2004; Bell et al., 2003; Koga et al., 2003; Kohlstedt et al., 1996; Litasov et al., 2007; Mosenfelder et al., 2006; Rauch and Keppler, 2002; Smyth et al., 2006), although values up to 1 wt.% H_2O cannot be excluded (Hirschmann et al., 2009).

With this in mind, the purpose of the present study is to employ an alternative and complimentary means of assessing mantle water content. To this end we make use of electromagnetic (EM) sounding, which has proved a valuable geophysical tool in addition to seismology for probing the physical structure of Earth's mantle (e.g., Kuvshinov, 2011). In spite of EM soundings having lower spatial resolution than do seismic methods, they are an important complement to the latter for extracting physical information, particularly on mantle water content through comparison of laboratory-based conductivity measurements of hydrous minerals with field estimates (e.g., Dai and Karato, 2009a,b,c; Huang et al., 2005; Manthilake et al., 2009; Wang et al., 2006; Yoshino et al., 2006, 2008a, 2009). Current laboratory-based conductivity measurements indicate average contents of ~0.01 wt.% H_2O in the upper mantle and ~0.1 wt.% H_2O in the TZ (e.g., Karato, 2011), although the possibility of a "dry" mantle cannot be excluded (e.g., Manthilake et al., 2009).

More to the point, knowledge of electrical conductivity by itself only provides hints about underlying properties. A more informative process comes from geophysically-derived conductivity models based on laboratory data following assumptions about composition and temperature (e.g., Dobson and Brodholt, 2000a; Fullea et al., 2011; Jones et al., 2009; Karato, 2011; Khan et al., 2011; Ledo and Jones, 2005; Pommier and Le Trong, 2011; Vacher and Verhoeven, 2007; Xu et al., 2000a). More definitive approaches in which EM data are inverted directly for thermochemical state (e.g., Khan et al., 2006; Verhoeven et al., 2009) are able to cover a much wider parameter range to be examined below.

In the first stage of this study we illustrate the sensitivity of EM sounding data to various properties (major element chemistry, temperature and water content) by comparing simple examples in which EM inductive responses of various conductivity profiles are constructed by varying in turn water content, composition, and temperature. In the next stage, we invert the EM sounding data for thermochemical state along the lines of a previous investigation (Khan et al., 2006) in which mineral phase equilibrium calculations based on Gibbs free energy minimization (Connolly, 2005) were interfaced with a stochastic sampling algorithm to generate a large collection of one-dimensional conductivity profiles whose EM responses are compared with geophysical observations. Here we consider four improvements: 1) a considerably augmented (in quantity and quality) mineral physics database of laboratory-measured electrical conductivities of upper mantle and TZ minerals obtained by two independent groups (e.g., Karato (2011) and Yoshino (2010)), which will be considered independently so as to minimize bias; 2) use of laboratory-measured water partition coefficients to realistically account for water allocation between various mineral phases; 3) high-quality long-period inductive responses recently acquired (Khan et al., 2011) from a set of geomagnetic observatories distributed across the globe (Europe, China, Australia, and North America); and 4) the possibility of thin hydrous fluid melt layers immediately above the TZ in cases where upper mantle water storage capacity is exceeded. Melt layers are a ubiquitous feature of the water filter hypothesis (Bercovici and Karato, 2003), and seismic evidence for low velocity zones above the TZ has been reported regionally (e.g., Revenaugh and Sipkin, 1994; Song et al., 2004; Tauzin et al., 2010). In view of the large conductivity increases associated with hydrous silicate melt (e.g., Mookherjee et al., 2008) these are potentially amenable of detection with EM sounding data (e.g., Park and Ducea, 2003; Shankland and Waff, 1977; Shankland et al., 1981; Toffelmier and Tyburczy, 2007).

2. Long-period electromagnetic sounding data

Data selection and processing have been described in detail in a previous study (Khan et al., 2011). Briefly, the *C*-responses (defined below) that we consider 1) satisfy quasi-1D behavior; 2) are located away from polar regions where auroral source effects are of possible influence (Fujii and Schultz, 2002); 3) have high coherency, low uncertainty, and vary smoothly; and 4) cover a large period range (3.9 to 95.2 days). The following stations were found to satisfy the above criteria: Fürstenfeldbrück (FUR), Europe; Langzhou (LZH), China; Alice Springs (ASP), Australia; Tucson (TUC), North America; Honolulu (HON), North Pacific; Hermanus (HER), South Africa. Of these we consider the first four stations for further analysis here, because the latter two are influenced by the ocean induction effect (Kuvshinov et al., 2002), which cannot be modeled thermodynamically. Length of data series and coordinates (geographical and geomagnetic) for the four stations are summarized in Table 1.

Under the assumption of a P_1^0 source structure, *C*-responses are defined as follows (Banks, 1969)

$$C(\omega) = -\frac{a\tan\vartheta}{2}\frac{Z(\omega)}{H(\omega)} \tag{1}$$

where $a = 6371.2$ km is Earth's mean radius, ϑ geomagnetic co-latitude, $Z(\omega)$ and $H(\omega)$ vertical and horizontal (directed toward geomagnetic

Table 1
Summary of geomagnetic observatories.

Station	Latitude	Longitude	Geomagnetic latitude	Observation period
Fürstenfeldbrück (FUR)	48.17	11.28	48.38	1957–2007
Langzhou (LZH)	36.09	103.85	25.86	1980–2007
Alice Springs (ASP)	−23.76	133.88	−32.91	1992–2007
Tucson (TUC)	32.17	249.27	39.88	1957–1994

north) components of the geomagnetic field, respectively, at frequency $\omega = 2\pi/T$ and period T. This technique is known as the $Z:H$ method (further details in Khan et al., 2011). As outlined in our previous investigation, the inductive responses provide information on mantle structure to a depth of about 1200 km and, although data are most sensitive in the depth range 500–1000 km, there is considerable sensitivity to upper mantle structure. The use of 1D radial conductivity profiles for making 3D inferences is also discussed in our previous study.

3. Laboratory electrical conductivity data

Experimental results show that mechanisms of mineral conductivity usually increase with temperature according to an Arrhenius relation (e.g., Tyburczy and Fisler, 1995)

$$\sigma = \sigma_0 exp\left(-\frac{H}{kT}\right) \tag{2}$$

where σ_0 is the so-called pre-exponential factor, H activation enthalpy, k Boltzmann's constant, and T is absolute temperature. σ_0 and H both depend on the particular charge transport mechanism. Generally, conductivity of a hydrous iron-bearing silicate mineral is given in terms of several charge transport mechanisms (e.g., Yoshino et al., 2009)

$$\sigma = \sigma_i + \sigma_h + \sigma_p \tag{3}$$

where σ_i, σ_h, and σ_p denote contributions from ionic conduction (migration of Mg-site vacancies), small polaron conduction (hopping of electrons between ferric and ferrous iron sites), and conduction arising from migration of protons, respectively.

Several groups have recently measured conductivity of major upper mantle and TZ minerals with the difficult outcome for the community of obtaining somewhat discrepant results. Whilst the issue has been debated (e.g., Karato, 2011; Karato and Dai, 2009; Yoshino, 2010; Yoshino and Katsura, 2009a), it is yet to be resolved. To minimize any particular bias we have created two electrical conductivity databases that are based on the measurements of 1) Yoshino, Katsura and coworkers (YK) and 2) Karato, Dai and coworkers (KD). These will be briefly summarized below.

Minerals of interest include olivine (ol), orthopyroxene (opx), clinopyroxene (cpx), garnet (gt), the high-pressure polymorph of cpx (C2/c), akimotoite (aki), wadsleyite (wad), ringwoodite (ring), ferropericlase (fp), perovskite (pv), calcium perovskite (ca-pv), and calcium ferrite (cf). It should be noted that in the case of C2/c, aki, ca-pv, and cf no conductivity measurements are presently available. As in Khan et al. (2006) we use the electrical conductivity of cpx as a proxy for C2/c and aki; for ca-pv we assume conductivity to equal that of Al-free pv, because Al is less soluble in ca-pv than in pv; for cf we disregard the contribution to conductivity in line with our earlier study (Khan et al., 2011), where it was shown that omitting the contribution of a mineral that is present at levels <10 vol.%, produces a difference in bulk conductivity of <0.02 log units. In the following we summarize the conductivity data employed here for the above minerals, and unless stated otherwise data parameters have the same meaning as in Eqs. (2)and (3). It should be noted that throughout we assume the mantle to be chemically homogeneous (compositional ranges investigated here are given in Table 10).

3.1. YK database

Electrical conductivity for hydrous iron-bearing olivine can be described by the form (Yoshino et al., 2009)

$$\sigma = \sigma_0^i \exp\left(-\frac{H_i}{kT}\right) + \sigma_0^h \exp\left(-\frac{H_h}{kT}\right) + \sigma_0^p C_w \exp\left(-\frac{H_0 - \alpha C_w^{1/3}}{kT}\right) \tag{4}$$

where the different σ_0s and Hs are pre-exponential factors and activation enthalpies for the various conduction mechanisms, respectively, C_w is water content in wt.%, and α a geometrical factor. Values for these parameters are given in Table 2.

For opx and cpx we model conductivity according to Eq. (2) and use the values for σ_0 and H measured by Xu and Shankland (1999). For gt we consider measurements by Yoshino et al. (2008a) and use Eq. (2) as in the case of opx and cpx. Parameter values are given in Table 3.

Wadsleyite conductivity is taken from Manthilake et al. (2009) and is given by

$$\sigma = \sigma_0^h exp\left(-\frac{H_h}{kT}\right) + \sigma_0^p C_w exp\left(-\frac{H_0 - \alpha C_w^{1/3}}{kT}\right) \tag{5}$$

where the first and second terms signify small polaron and proton conduction, respectively. Parameter values are summarized in Table 4.

For ringwoodite, we consider the measurements by Yoshino et al. (2008b) for proton conduction, while the small polaron term is taken from Yoshino and Katsura (2009b).

$$\sigma = \sigma_0^p C_w exp\left(-\frac{H_0 - \alpha C_w^{1/3}}{kT}\right) + \sigma_0^{Fe} X_{Fe} exp\left(-\frac{H_0^{Fe} - \alpha_{Fe} X_{Fe}^{1/3}}{kT}\right). \tag{6}$$

In the Fe correction term, X_{Fe} is mole fraction of Fe in the Mg site, H_0^{Fe} activation enthalpy at very low Fe concentrations, and α_{Fe} a geometrical factor; Yoshino and Katsura (2009b) found two different temperature regimes each with their own parameter values. Parameter values are compiled in Table 5.

For the major lower mantle minerals ferropericlase and perovskite electrical conductivities are modeled as

$$\sigma = \sigma_0 exp\left(-\frac{E + PV}{kT}\right) \tag{7}$$

where E, P and V are activation energy, pressure, and activation volume respectively. These parameters were measured by Xu et al. (2000a) for ferropericlase and Xu et al. (1998) for both Al-free and Al-bearing perovskite. Data parameters are tabulated in Table 6.

In treating upper mantle and transition zone minerals we have omitted pressure effects arising from activation volumes because of the relatively narrow pressure ranges over which the minerals are stable. Although some laboratory experiments have suggested that conductivity of major lower mantle minerals varies with composition (Fe in the case of ferropericlase (Dobson and Brodholt, 2000b; Wu et al., 2010) and Al in the case of perovskite (Xu et al., 1998)), we omit

Table 2
Parameter used to characterize olivine conductivity (after Yoshino et al., 2009).

log_{10} (σ_i)	H_i (eV)	log_{10} (σ_0^h)	H_h (eV)	log_{10} (σ_0^p)	H_0 (eV)	α
4.73 ±0.53	2.31 ±0.07	2.98 ±0.85	1.71 ±0.04	1.9 ±0.44	0.92 ±0.04	0.16 ±0.02

Table 3
Parameters used to characterize conductivities of orthopyroxene (opx), clinopyroxene (cpx) and garnet (gt). For gt no uncertainties were provided in the original data. Parameters are from Xu and Shankland (1999) for opx and cpx, and Yoshino et al. (2008a) for gt.

Mineral	log_{10} (σ_0)	H (eV)
opx	3.72 ± 0.1	1.8 ± 0.02
cpx	3.25 ± 0.11	1.87 ± 0.02
gt (<1300 K)	1.73	1.27
gt (1300–1750 K)	3.03	1.59
gt (>1800K)	4.24	2.02

their possible contributions here, given that geophysical data only sense to depths of ~1200 km.

3.2. KD database

Conductivity data from Karato, Dai and coworkers (Dai and Karato (2009a,b,c), Huang et al. (2005), Wang et al. (2006)) are taken from a recent review (Karato, 2011) and include measurements of ol, opx, gt, wad, and ring. Electrical conductivity of these minerals was described by a relationship of the form

$$\sigma = A_1 \exp\left(-\frac{E_1 + PV_1}{RT}\right) + A_2 C_w^r \exp\left(-\frac{E_2 + PV_2}{RT}\right) \quad (8)$$

where A is a pre-exponential factor, C_w water content in wt.%, r an exponent determining water dependence, E activation energy, P pressure, V activation volume, T temperature, and R the gas constant; subscripts 1 and 2 refer to mechanisms of polaron (1) and proton (2) conduction. Note that effects of oxygen fugacity (f_{O_2}) have been omitted because f_{O_2} is not well-constrained and uncertainties are likely to be small compared to those arising from other parameters (further discussed in next section). The various parameters are tabulated in Table 7. For lower mantle minerals we employ equations and parameters summarized in the previous section.

3.3. Mineral water partition coefficients

We consider partitioning of water between the following minerals for which conductivity measurements under hydrous conditions exist: orthopyroxene/olivine and garnet/olivine. For orthopyroxene/olivine we employ a partition coefficient $\left(D_{H_2O}^{opx/ol}\right)$ of 15, based on the measurements of Aubaud et al. (2004), Grant et al. (2004), Hauri et al. (2004) and Koga et al. (2003). For garnet/olivine we use $D_{H_2O}^{gt/ol} = 2$ from results of Hauri et al. (2004). Experiments on the partitioning behavior of water between wadsleyite and olivine have also been carried out, but are not used here as we want to determine water content of the upper mantle and transition zone independently of each other. In the TZ we invoke the simplifying assumption that $D_{H_2O}^{ring/wad} = 1$ (see also Section 7.1.4). The partitioning behavior between lower mantle minerals is not of interest as conductivity measurements on hydrous lower mantle minerals currently are not available.

Table 4
Wadsleyite conductivity parameters and their sources (after Manthilake et al., 2009).

σ_0^h (S/m)	H_h (eV)	σ_0^p (S/m)	H_0 (eV)	α
399 ± 311	1.499 ± 0.1	7.749 ± 4.08	0.689 ± 0.03	0.02 ± 0.02

3.4. Mineral water storage capacity and melt layer on top of the TZ

The water storage capacities of mantle minerals of interest here include those of olivine and wadsleyite. Given current uncertainties in the storage capacity of the upper mantle (e.g., Hirschmann et al., 2005, 2009), which ranges from 0.05 to 0.5 wt.%, we employ a value of 0.1 wt.% H_2O (Férot and Bolfan-Casanova, submitted for publication). For wadsleyite we assume an upper bound of ~3 wt.% based on the considerations of Smyth (1987) and the measurements of Bolfan-Casanova et al. (2000), Inoue et al. (1995) and Kohlstedt et al. (1996). This value is likely to be slightly on the high side, given measurements by Demouchy et al. (2005) that showed Fe-bearing wadsleyite to contain 2.5 wt.% H_2O at 1400 °C and to decrease to 1.5 wt.% at ~1500 °C (see also discussion by Bolfan-Casanova, 2005). We assume water storage in the TZ to be controlled by the solubility of wadsleyite, since majorite garnet contains <0.1 wt.% H_2O (e.g. Bolfan-Casanova et al., 2006). Although there is evidence that olivine water content decreases as a function of pressure and temperature above 5 GPa and 1100 °C (Peslier et al., 2010), we assume that water storage capacity is independent of temperature and pressure because of limited experimental data and sensitivity of EM sounding data.

The importance of specifically considering bounds on the water storage capacity of olivine and wadsleyite stems from the observation that hydrous melting ensues at locations where the upper mantle water content, assumed to be controlled principally by that of olivine given its larger volume fraction in comparison to garnet and orthopyroxene, exceeds the local storage capacity. This likely occurs in the shallow mantle within the basalt source regions (e.g., Kohlstedt et al., 1996) and, of more relevance for the present case, in the deep part of the upper mantle when material enriched in water is advected from the TZ (e.g., Bercovici and Karato, 2003). Specifically, we employ the storage capacity of olivine discussed above as a threshold value above which we assume that a melt layer of a given thickness and conductivity appears, in line with the modeling assumptions of Toffelmier and Tyburczy (2007). These simplifying assumptions are warranted given the generally unknown composition of such a hydrous silicate melt, the currently limited database of electrical conductivity measurements associated with melts, and absence of information on melt configuration, i.e., interconnectedness, within the layer, which is important if melt conductivity is to dominate that of the resistive solid matrix (e.g., Shankland and Waff, 1977). Further details on physical properties describing the melt layer are in Section 7.1.5.

3.5. Oxygen fugacity and miscellaneous effects

Most of the above experiments were made at oxygen fugacities controlled by the Mo-MoO_2 buffer (Table 2 of Karato (2011) contains a summary of oxygen fugacities associated with the most recent conductivity experiments). Although it has been observed that olivine conductivity could vary as $f_{O_2}^{1/6}$ (Duba and Constable, 1993; Schock et al., 1989), effects of f_{O_2} under mantle conditions are weakly quantified (Xu et al., 2000b). As a result we make no oxygen fugacity corrections to conductivity of the mantle minerals considered here and thus make the assumption that f_{O_2} throughout the mantle is near that of the Mo-MoO_2 buffer. Moreover, as assessed by Karato (2011), the influence of f_{O_2} on conductivity profiles computed in that study is relatively small given that oxygen fugacity itself varies relatively little. This is also observed when computing conductivity of olivine for various oxygen fugacities using SIGMELTS (Pommier and Le Trong, 2011).

Pressure effects on electrical conductivity of upper mantle minerals have been investigated by Xu et al. (2000b) for olivine and by Dai and Karato (2009a) for pyrope garnet. Resulting effects were observed to be weak in the work of Xu et al. particularly in the depth range 80–200 km, while at 400 km depth olivine conductivity changed by less than a factor of 2.5 when varying activation volumes ± 0.6 cm^3/

Table 5
Ringwoodite conductivity parameters and their sources. The small polaron term is from Yoshino and Katsura (2009b), whereas the proton conduction term is from Yoshino et al. (2008b).

T (K)	σ_0^p (S/m)	H_0 (eV)	α	σ_0^{Fe} (S/m)	H_0^{Fe} (eV)	α_{Fe}
<1000	27.79 ± 9.6	1.12 ± 0.03	0.67 ± 0.03	467 ± 150	2.14 ± 0.05	2.14 ± 0.07
>1000	27.79 ± 9.6	1.12 ± 0.03	0.67 ± 0.03	10,042 ± 4211	2.08 ± 0.06	1.55 ± 0.09

mol. Based on these results we neglect the effect of pressure on upper mantle conductivity here.

As in Xu et al. (2000a) and our previous studies no corrections were made for grain boundary effects, given that substantial systematic variations in conductivity are yet to be observed (e.g., Dai et al., 2008; Duba and Shankland, 1982; Roberts and Tyburczy, 1993; ten Grotenhuis et al., 2004; Watson et al., 2010; Xu et al., 2000a).

Contributions to bulk electrical conductivity of some minor mineral phases are not accounted for because of a lack of relevant laboratory measurements. However, disregarding contributions from phases that are present at levels of ~10 vol.% amounts to a negligible difference in bulk conductivity. Specifically, Khan et al. (2011) found that omitting the contribution from the C2/c (high-pressure polymorph of cpx) phase, for example, resulted in a difference of <0.02 log-units, which for practical purposes is insignificant.

Finally, no exhaustive attempt to consider other data sets, e.g., measurements by Romano et al. (2006) on garnet, Romano et al. (2009) on hydrous wadsleyite, Poe et al. (2010) on hydrous olivine, or Wu et al. (2010) on ferropericlase was made and the choice of experimental data possibly influences the outcome. However, because this inversion treatment is able to consider uncertainties in measured conductivity parameters, it automatically allows for larger variations, and we are thus a priori less likely to bias the results.

4. Thermodynamic modeling

In order to compute mantle mineral modes for a given composition X and temperature T, we assume mantle mineralogy to be governed by thermodynamic equilibrium and predict mineralogy as a function of composition, pressure, and temperature by Gibbs energy minimization using the self-consistent method of Connolly (2005). We adopt the thermodynamic formalism of Stixrude and Lithgow-Bertelloni (2005) as parameterized by Xu et al. (2008) for mantle minerals in the model chemical system Na_2O–CaO–FeO–MgO–Al_2O_3–SiO_2 (abbreviated NCFMAS). The Gibbs energy minimization procedure yields amounts, compositions, and physical properties, including elastic moduli, of the stable minerals in the model chemical system.

5. Laboratory-based electrical conductivity models

With the data described above we can construct aggregate mantle conductivity profiles. It is necessary to average conductivities of individual minerals with their volume fractions, and there are several different schemes to do this in the absence of information on the actual distribution of various mineral phases within the bulk rock.

Table 6
Parameters used to model ferropericlase (fp) and perovskite (pv) conductivities. Parameters are from Xu et al. (2000a) for fp and Xu and Shankland (1999) for pv.

Mineral	log_{10} (σ_0)	E (eV)	V (cm^3/mol)
fp	2.69 ± 0.1	0.85 ± 0.03	−0.26
pv (Al-bearing)	1.87 ± 0.11	0.7 ± 0.04	−0.1
pv (Al-free)	1.12 ± 0.12	0.62 ± 0.04	−0.1

Of general utility for the calculation of conductivity for multiphase materials are some generalized averages, which include the arithmetic (A) mean (Voigt average), and the harmonic (H) mean (Reuss average)

$$\sigma_A = \sum_i^N x_i \sigma_i, \quad \sigma_H = \left[\sum_i^N \frac{x_i}{\sigma_i} \right]^{-1} \tag{9}$$

where σ_i and x_i are conductivity and volume fraction of mineral phase i, respectively, and N is the total number of mineral phases present. The above averages are extremes for upper and lower bounds of bulk conductivity and bracket the permissible range within which the effective conductivity of the multiphase system must be contained (e.g., Park and Ducea, 2003; Waff, 1974). It is implicitly assumed that x_i is a function of composition, pressure, and temperature, whereas σ_i depends on pressure and temperature as well as Fe and H_2O content.

Hashin–Shtrikman bounds are considered the narrowest upper and lower bounds for a multiphase system in the absence of knowledge of the geometrical arrangement of the constituent phases (Berryman, 1995; Hashin and Shtrikman, 1962; Watt et al., 1976). The lower bound (HS−) assumes non-interconnected conductive inclusions within a resistive matrix, and the upper bound (HS+) assumes non-interconnected resistive inclusions in a conductive matrix

$$\sigma_{\mathrm{HS}\pm} = \left[\sum_{i=1}^N \frac{x_i}{\sigma_i + 2\sigma_\pm} \right]^{-1} - 2\sigma_\pm \tag{10}$$

where σ_i and x_i are as before conductivity and volume fraction of mineral phase i, respectively, and $\sigma_\pm$ correspond to minimum ($\sigma_- = min(\sigma_i)$) and maximum ($\sigma_+ = max(\sigma_i)$) conductivities of the N mineral phases.

In addition to computing bounds we also compute estimators. We consider 1) the geometric mean, 2) the effective medium theory of Landauer (1952) for conducting composites and generalized by Berryman (1995), and 3) the Hill or the Voigt–Reuss–Hill average (Hill, 1963; Watt et al., 1976). The latter average (σ_{VRH}) is the arithmetic mean of the Voigt and Reuss bounds and is biased toward the Voigt bound (Shankland and Duba, 1990). The geometric mean (GM) used previously by Shankland and Duba (1990) can readily be computed (e.g., Constable, 2006)

$$\sigma_{\mathrm{GM}} = \prod_i \sigma_i^{x_i}. \tag{11}$$

Table 7
Parameters taken from Karato, Dai and coworkers (Karato, 2011) used for modeling conductivity of olivine (ol), orthopyroxene (opx), garnet (gt), wadsleyite (wad) and ringwoodite (ring). Parameter uncertainties are ±10 kJ/mol for E, ±0.1 for r and ±0.1/0.3 (polaron/proton) for $log_{10}A$.

Mineral	$log_{10}A_1$	$log_{10}A_2$	r	E_1/E_2 (eV)	V_1/V_2 (cm^3/mol)
ol	2.4	3.1	0.62	154/87	2.4/−
opx	2.7	2.6	0.62	147/82	−/−
gt	2.1	2.7	0.63	128/70	2.5/−0.6
wad	2.1	2.1	0.72	147/88	−/−
ring	–	3.6	0.69	−/104	−/−

With more computational effort effective medium theory produces a self-consistent solution (σ_{sc}) that is found through iteration to satisfy (while being bounded by HS− and HS+)

$$\sum_{i=1}^{N} x_i \left[\frac{\sigma_i - \sigma_{sc}}{\sigma_i + 2\sigma_{sc}} \right] = 0. \tag{12}$$

The various conductivity bounds and estimates are illustrated in Fig. 1 for pyrolite composition along the geotherm of Brown and Shankland (1981) using the YK conductivity database at "dry" mantle conditions. We observe, as in Shankland and Duba (1990), that the only estimator consistently within the Hashin–Shtrikman bounds is σ_{sc}; both σ_{GM} and σ_{VRH} can lie outside these bounds at various points along the bulk conductivity profile. As Hashin–Shtrikman bounds present the narrowest possible restrictions that exist on an arbitrary isotropic multi-phase system, we consider, like Xu et al. (2000a), self-consistently determined conductivity values as the most appropriate average bulk rock conductivity.

Prior to inverting data, we treat some simplified forward models to investigate to what extent the various properties (major element chemistry, temperature, and water content) influence electrical conductivity and, most importantly, *C*-responses. This approach helps indicate the main consequences of the two databases.

6. Variation in mantle material properties

6.1. Water content

For modeling purposes we consider a homogeneous adiabatic mantle of pyrolite composition (Table 9) using the mantle adiabat of Brown and Shankland (henceforth BS adiabat). With this background model, we vary mantle water content for both conductivity databases using the C_ws given in Table 8 and compute bulk rock conductivity profiles from the equilibrium mineralogy obtained via Gibbs free energy minimization outlined in Section 4. The resulting variations in phase proportions and aggregate conductivity for the two databases are shown in Fig. 2.

For the YK database conductivity variations in the upper mantle are negligible, whereas differences in the upper and lower TZ are ~0.3 and ~0.01 log-units, respectively. Minor conductivity variations in the lower TZ are related to the small contribution arising from the proton conduction term relative to the polaron term (Eq. (6)). In contrast, the KD database produces strong conductivity variations in the upper mantle that reach 0.5–1 log-unit, with even stronger variations occurring in the TZ. Comparison of the YK and KD conductivity profiles further accentuates these first-order differences. For the "dry" case, YK is overall more conductive than is KD, with a conductivity decrease across the ol→wad (410-km seismic discontinuity), while KD shows an increase at the same location in addition to a large jump (~2.5 log-units) at the transition ring→fp+pv (660-km). For the other two "wet" cases the KD conductivity profiles are generally more conductive than the YK profiles over the entire depth range considered here, with relatively strong "410"s and no "660"s, while for the YK profiles the "660" is the strongest transition (0.5–0.6 log-units). Fig. 2 illustrates the important point that in the TZ the KD database requires a smaller water content than does the YK database to achieve the same conductivity increase. With the YK database this appears in the inversion results as requiring a greater water content at the bottom of the upper mantle than does the KD database. For pressures >25 GPa (corresponding to depths >700 km) the different mantle conductivity profiles converge as expected, because the two databases use the same conductivity data for the lower mantle. Inductive response functions for the six conductivity profiles of Fig. 2 are shown in Fig. 3, and we note that while the YK conductivity profiles are almost indistinguishable within the uncertainties of the data, the KD profiles are easily differentiated. For brevity here and in the following two subsections (6.2 and 6.3) only the real part of the inductive response is shown.

Simplifying assumptions made in the present exercise include, in addition to neglecting the contribution from minor mineral phases as discussed previously, disregarding the effect of water on mineral phase equilibria. Although there is evidence from theory and experiment that water is likely to stabilize wadsleyite over olivine thereby decreasing depth to the 410-km discontinuity (e.g., Chen et al., 2002; Smyth and Frost, 2002; Wood, 1995), scarcity of relevant

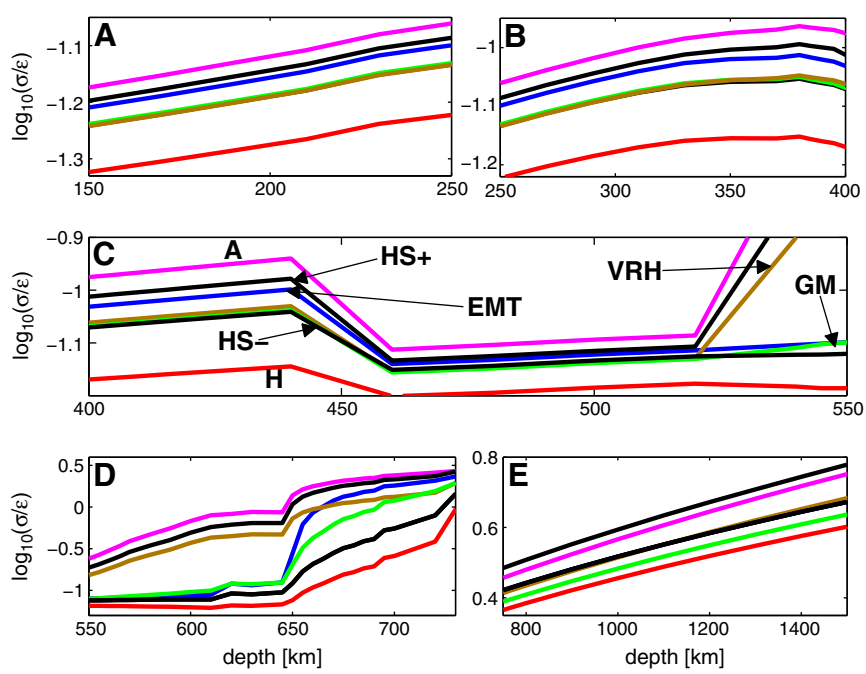

Fig. 1. Estimated bulk conductivity profiles using different averaging schemes (see main text for details) in the upper mantle (A,B), transition zone (C,D) and lower mantle (E). Color coding is the same in all plots. The following averages are shown: A — arithmetic mean; H — harmonic mean; HS — lower Hashin–Shtrikman bound; HS+ — upper Hashin–Shtrikman bound; EMT — effective medium theory; VRH — Voigt–Reuss–Hill average; and GM — geometric mean. In (a) and (b) HS− is hidden behind the GM and VRH profiles. $\varepsilon = 1$ S/m.

Table 8
Water contents used for modeling electrical conductivities; water contents are in wt.%. Labels a–c are used to identify the conductivity profiles in Fig. 2. Note that KD provided no conductivity data for ringwoodite at "dry" conditions, and 0 wt.% actually implies the presence of a minute amount of water (0.0001 wt.%).

Database	C_w^{ol}	C_w^{opx}	C_w^{gt}	C_w^{wad}	C_w^{ring}
YK(a)	0	–	–	0	0
YK(b)	0.001	–	–	0.1	0.1
YK(c)	0.005	–	–	0.5	0.5
KD(a)	0	0	0	0	0
KD(b)	0.001	0.001	0.001	0.1	0.1
KD(c)	0.005	0.005	0.005	0.5	0.5

thermodynamic data prevents us from including this effect. However, given the modest change in conductivity across the ol → wad transition, this is likely a minor issue.

6.2. Major element composition

We consider three different "dry" mantle compositions: 1) harzburgite, 2) pyrolite, and 3) basalt. The compositions are tabulated below (Table 9). As before we compute the equilibrium mineralogies for each of these compositions using Gibbs free energy minimization along the BS adiabat. The resulting electrical conductivities are shown in Fig. 4.

The distinction between computed conductivity profiles is clearly noticeable, which is a direct consequence of the different stable mineralogies produced for each of the three compositions. Again, KD profiles are overall more conductive than their YK counterparts. For the latter, strong conductivity increases only occur at pressures around 18–20 GPa (520-km seismic discontinuity) and ~23 GPa (660-km). Fig. 4 also shows *C*-responses computed from the six profiles that are distinguishable within the uncertainties of the EM sounding data.

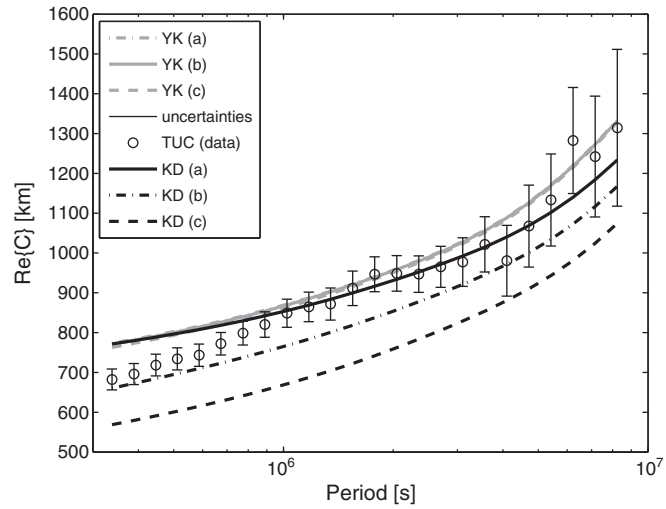

Fig. 3. Inductive response functions (real part only) calculated for the six conductivity profiles shown in Fig. 2 and compared to observations from station TUC. KD and YK refer to the laboratory databases used for modeling conductivity profiles. (a), (b), and (c) refer to the same compositions as in the previous figure.

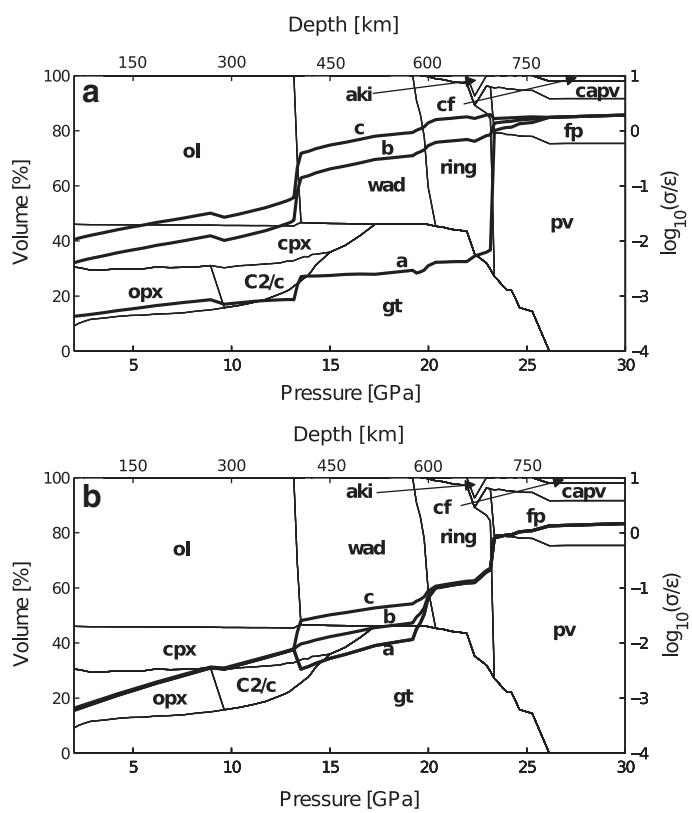

Fig. 2. Bulk conductivity profiles as a function of water content in the upper mantle, transition zone, and uppermost lower mantle. Conductivity profiles in plots (A) and (B) were constructed using the KD and YK conductivity databases, respectively. In both plots water content in the upper mantle (UM) and transition zone (TZ) is: (a) both 0 wt.% water, i.e., "dry" conditions, (b) 0.001 wt.% (UM), and 0.1 wt.% (TZ) and (c) 0.005 wt.% (UM) and 0.5 wt.% (TZ). Note that the KD database does not contain a conductivity term for ringwoodite at "dry" conditions; for these calculations we included a vanishingly small amount of water (0.0001 wt.%). Equilibrium mineralogy is computed on the basis of a pyrolitic mantle composition and an adiabatic temperature profile (see main text for details). Phases are (mineral abbreviations defined in the main text): ol, opx, cpx, C2/c, gt, wad, ring, aki, ca-pv, fp, pv, and cf. $\varepsilon = 1$ S/m.

Table 9
Model endmember bulk compositions in wt.%. Basalt and harzburgite compositions are from Khan et al. (2009), whereas the pyrolite composition is taken from Lyubetskaya and Korenaga (2007).

Component	Basalt	Harzburgite	Pyrolite
CaO	13.05	0.5	2.79
FeO	7.68	7.83	7.97
MgO	10.49	46.36	39.5
Al_2O_3	16.08	0.65	3.52
SiO_2	50.39	43.64	44.95
Na_2O	1.87	0.01	0.298

6.3. Geotherm

We consider a homogeneous mantle of pyrolitic composition and combine it with three different geotherms: 1) the BS adiabat (T_{BS}), 2) a "subadiabat" (T_{BS}-150 K), and 3) a "superadiabat" ($T_{BS}+150$ K). Again we assume a "dry" mantle and compute for each of the geotherms bulk electrical conductivity profiles and inductive response functions (Fig. 5).

As expected, in the upper mantle there is a quasi-linear variation in conductivity with temperature, given similarity in equilibrium mineralogy among the three different models. This contrasts with the TZ and uppermost lower mantle, where conductivity changes are no longer simply proportional to temperature. Conductivity is seen to vary by ~0.4 to 1 log-unit in the upper mantle and by ~ 0.2–0.3 log-units in the TZ. For a given geotherm KD-based profiles are more conductive than their YK counterparts. KD-based profiles are distinguished by a strong conductivity increase at the ol→wad transition (~13 GPa), whereas such a transition is almost absent in YK-based profiles. The opposite occurs at ~18 GPa (wad→ring transition at ~520-km) and at ~23 GPa (ring→fp+pv), where the YK profiles display much stronger increases than do the KD profiles. Electromagnetic response functions for the six profiles are also shown in Fig. 5 and appear to be distinguishable within uncertainties of response functions.

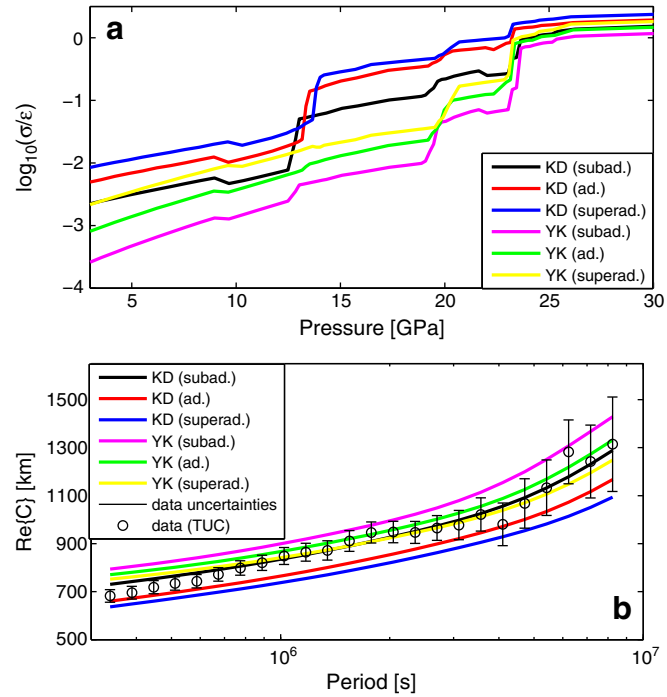

Fig. 5. Dependence of conductivity and response functions on mantle geotherm. (a) Bulk conductivity profiles for three different geotherms, comprising "subadiabatic", adiabatic, and "superadiabatic" mantle conditions from the lithosphere down to the outermost lower mantle using the conductivity databases KD and YK. $\varepsilon=1$ S/m. (b) Inductive response functions (real part only) for the six profiles shown in (a) and compared to observations from station TUC. "Dry" mantle conditions are assumed.

In summary, these forward-modeling tests have revealed perceptible differences between the two electrical conductivity databases. Most notably, conductivity profiles constructed from the KD-based database are generally more conductive than their YK-

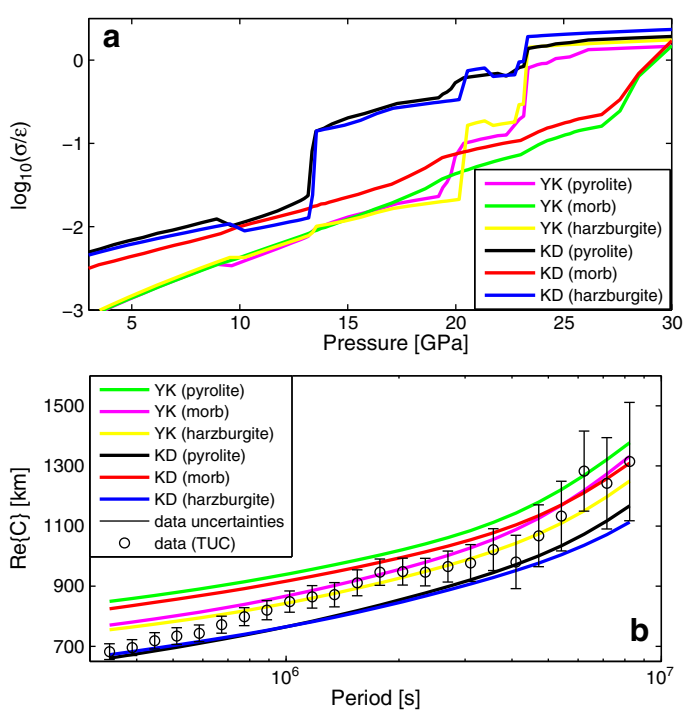

Fig. 4. Dependence of conductivity and response functions on mantle composition. (a) Bulk conductivity profiles for three different compositions in the upper mantle, transition zone, and outermost lower mantle (Table 9) using the two conductivity databases KD and YK. $\varepsilon=1$ S/m. (b) Inductive response functions (real part only) for the six profiles shown in (a) and compared to observations from station TUC. "Dry" mantle conditions are assumed.

based counterparts for a given set of conditions (water content, chemical composition, thermal state). In particular, KD-based conductivity profiles respond strongly to changes in water content. In comparison, YK conductivity profiles appear generally insensitive to changes in upper mantle and lower TZ water content. Another noticeable difference is the strength of the discontinuous changes in conductivity at major mantle phase transitions. KD-based conductivity profiles generally show strong changes in conductivity at the "410", whereas YK conductivity profiles display relatively strong "520"s and "660"s.

7. Inverse modeling

This section outlines the methodology used to invert the long-period EM sounding data for mantle composition, temperature, and water content. We closely follow the approach of Khan et al. (2006, 2007) which supply details.

In an inverse problem the relationship between model **m** and data **d** is usually written as

$$\mathbf{d} = \mathrm{g}(\mathbf{m}) \tag{13}$$

where g in the general case is a non-linear operator. However, there is a problem in the absence of an analytical expression for g that would allow us to compute inductive response functions from a knowledge of mantle composition, temperature, and water content. In place of an analytical expression we use an algorithm that, when applied to the various parameters, is able to compute the desired response functions. The workings of the algorithm are given in the scheme below and shows the complete solution of the forward problem

$$\{X, T, C_w\} \xrightarrow{\mathrm{g}_1} \{M\} \xrightarrow{\mathrm{g}_2} \{\sigma\} \xrightarrow{\mathrm{g}_3} \{\mathrm{Re}(C), \mathrm{Im}(C)\}$$

where X, T and C_w are the fundamental parameters sought, M is equilibrium modal mineralogy, σ is bulk conductivity profile, Re(C) and Im(C) real and imaginary parts of inductive response, respectively. The different g's denote the various physical laws, i.e., Gibbs free energy minimization (g_1), construction of bulk laboratory-based conductivity profile (g_2), and prediction of data (g_3).

Central to formulation of a Bayesian approach to inverse problems is extensive use of probability density functions (*pdf*'s) to delineate parameters specific to the problem (Tarantola and Valette, 1982). These include probabilistic prior information on model and data parameters, $f(\mathbf{m})$ (for the present discussion we limit ourselves to a functional dependence on **m** and omit any reference to **d**), and the physical laws that relate data to the unknown model parameters. Using Bayes's theorem these *pdf*'s are combined to yield the posterior probability density function in the model space

$$\sum(\mathbf{m}) = kf(\mathbf{m})\mathcal{L}(\mathbf{m}), \tag{14}$$

where k is a normalization constant and $\mathcal{L}(\mathbf{m})$ is the likelihood function, which in probabilistic terms can be interpreted as a measure of misfit between observations and predictions from the model **m**.

We use the Metropolis algorithm (a Markov chain Monte Carlo method) to sample the posterior distribution in the model space using the approach of Mosegaard and Tarantola (1995). While this algorithm is based on a random sampling of the model space, only models that result in a good data fit and that are consistent with prior information are frequently sampled.

Due to the generally complex shape of the posterior distribution, typically employed measures such as means and covariances are generally inadequate descriptors. Instead we present the solution in terms of a large collection of models sampled from the posterior probability density. In the following section we describe prior information, parameterization, and the likelihood function.

7.1. Prior information

We consider a spherical Earth varying laterally and radially in properties. At the location of each geomagnetic observatory at the Earth's surface, we represent a (local) model of the Earth by a number of layers, corresponding to crust and mantle layers (details given below). The crust is represented by a local physical model, whereas mantle layers are described by model parameters related to composition and temperature. It is implicitly assumed that all parameters depend on geographical position and depth.

7.1.1. Crust

As the long-period EM sounding data considered here are only marginally sensitive to crustal structure we use a simplified parameterization consisting of a crust with the Moho fixed at 50 km depth beneath each station. Crustal conductivity (σ_{cr}) varies independently among the various sites with an interval of 10^{-6} S/m to 10^{-3} S/m and is made to increase with depth down to the Moho.

7.1.2. Mantle composition

We model the mantle composition using the Na_2–CaO–FeO–MgO–Al_2O_3–SiO_2 (NCFMAS) model system, that accounts for more than 98% of mass of the mantle (Irifune, 1994). Mantle composition is assumed to be uniformly distributed within the bounds given in Table 10.

Bounds are chosen such that compositions agree with the range of compositions of mantle peridotites derived from several geochemical studies (Table 2 of Lyubetskaya and Korenaga (2007)).

7.1.3. Temperature

We assume mantle temperature to be uniformly distributed with no lower or upper bounds, except for a constant surface temperature of 0 °C. We additionally require that temperature not decrease as a function of depth and employ the constraint $T_{j-1} \le T_j \le T_{j+1}$ where T_j is temperature in layer j. In this scheme we determine temperature in 25 uniform layers at intervals of 50 km in the depth range 0–700 km and 100 km in the range 700–2886 km; this yields 26 thermal parameters.

7.1.4. Mantle water content

We model water content in the following minerals: olivine, orthopyroxene, garnet, wadsleyite, and ringwoodite and use the simplifying assumption that $C_w^{\mathrm{wad}} = C_w^{\mathrm{ring}}$, because of data sensitivity in the mantle TZ (Khan et al., 2011), in addition to the use of water partition coefficients as discussed in Section 3.3. The latter implies that only C_w^{ol} and C_w^{wad} need to be determined. Furthermore, we assume that C_ws for all the above minerals are log-uniformly distributed within intervals in the range 0–0.1 wt.% (olivine) and 0–3 wt.% (wadsleyite) H_2O, respectively. As the KD conductivity measurements do not include measurements for purely "dry" ringwoodite, i.e., a polaron term in Eq. (8) is absent, we set a lower limit of 10^{-4} wt.% H_2O for C_w^{TZ}(KD).

7.1.5. Melt layer conductivity

In view of the unknown composition of hydrous silicate melts and scarcity of electrical conductivity measurements pertaining to such melts (e.g., Gaillard, 2004; Maumus et al., 2005; Ni et al., 2011;

Table 10
Model compositions in wt.%.

Component	Mantle
CaO	2.32–3.88
FeO	7.24–8.84
MgO	35–41.6
Al_2O_3	2.92–4.87
SiO_2	40.5–49.4
Na_2O	0.16–0.44

Pommier et al., 2010; Roberts and Tyburczy, 1999; Tyburczy and Waff, 1983; Yoshino et al., 2010), we consider a melt layer with a fixed thickness of 20 km and conductivity that varies from the "background" mantle value (σ_m) and up to a maximum of $2+\sigma_m$ (S/m), i.e., $\sigma_{melt}=\sigma_m+2\cdot\alpha$, where α is a randomly distributed number in the interval 0–1. For comparison, Toffelmier and Tyburczy (2007) used values of 1–6 S/m for the conductivity of their melt layer (5–30 km thick) based on low-pressure conductivity measurements of various melts, including basanite melt, olivine tholeiitic melt, "dry" and "wet" rhyolitic melt, Yellowstone rhyolite and Hawaiian tholeiite (Gaillard, 2004; Tyburczy and Fisler, 1995; Tyburczy and Waff, 1983) and an assumed temperature at the 410-km discontinuity of around 1420 °C.

7.1.6. Electrical conductivity parameters

Uncertainties in all parameters relevant to modeling conductivity (e.g., $\sigma_0, H, \alpha, A, r, E$ — see Tables 2–7), are considered by assuming that these are uniformly distributed within bounds of $[p-\Delta p; p+\Delta p]$, where p is any of the aforementioned parameters and Δp the associated uncertainty.

7.1.7. Modal mineralogy and bulk electrical conductivity

Being secondary parameters, i.e., conditional on the values of X, T and C_w, no prior constraints apply to M and σ. This also applies to the conductivity structure of the mid- and lower mantle where data lack sensitivity; core conductivity was fixed to $5\cdot10^5$ S/m (Stacey and Anderson, 2001).

7.1.8. Overall parameterization

In summary, given values of the parameters described above we compute equilibrium modal mineralogy and bulk conductivity at 75 depth nodes from the surface downward as a function of pressure, temperature, and composition at intervals of 10 km in the range 50–110 and 570–630 km depth, 20 km in the ranges 110–370, 420–540 and 700–800 km depth, 5 km within the range 380–420, 545–570 and 645–700 km depth, 100 km in the range 800–1600 km depth, and finally 200 km in the depth range from 1600 to 2000 km.

There is no unique way to parameterize the model system, and the particular parameterization chosen here has been found by conducting many trial inversions and reflects a particular, near-minimal, parameterization that yields data fitting the observations within uncertainties. Also, as we have neglected uncertainties of measured mineral physics parameters related to the thermodynamic formulation, actual uncertainties are likely larger than indicated here.

7.2. Posterior distribution

Assuming that data noise can be modeled using a Gaussian distribution and that observational uncertainties and calculation errors between the real and imaginary part of the C-response functions are independent, the likelihood function is given by

$$\mathcal{L}(\mathbf{m})\propto exp\left(-\sum_i \frac{\left[{}_id_{obs}^{\mathrm{Re}\{C\}}-{}_id_{cal}^{\mathrm{Re}\{C\}}(\mathbf{m})\right]^2}{2{}_i\Delta^2_{\mathrm{Re}\{C\}}}+\frac{\left[{}_id_{obs}^{\mathrm{Im}\{C\}}-{}_id_{cal}^{\mathrm{Im}\{C\}}(\mathbf{m})\right]^2}{2{}_i\Delta^2_{\mathrm{Im}\{C\}}}\right) \quad (15)$$

where $d_{obs}^{\mathrm{Re}\{C\}}$, $d_{obs}^{\mathrm{Im}\{C\}}$, $d_{cal}^{\mathrm{Re}\{C\}}$ and $d_{cal}^{\mathrm{Im}\{C\}}$ denote observed and calculated real and imaginary C-responses, respectively, and $\Delta_{\mathrm{Re}\{C\}}$ and $\Delta_{\mathrm{Im}\{C\}}$ are the observational uncertainties on either of these.

Sampling proceeded by randomly perturbing either of the parameters in the set $\{X, T, C_w, \sigma_{cr}\}$ according to the prior distribution as defined in Section 6.1 (for brevity we leave aside parameters pertaining to measurement uncertainties ($\sigma_0, A, H, \alpha, E, V$). The burn-in time for this distribution (number of iterations until samples were retained from the posterior distribution) was found to be of the order of $5\cdot10^4$. We sampled 1 million models, with an overall acceptance rate of about 35% of which every 100th model was retained for further analysis.

8. Results and discussion

8.1. Thermal structure

Fig. 6 shows the retrieved thermal structure beneath the four stations and reveals mantle temperatures that span a range of 200–250 °C to a depth of about 800–900 km. Generally, we observe that sampled geotherms remain relatively well-defined in comparison to prior models over most of the depth range shown here. Comparison of the various thermal profiles obtained from inversion of the two databases is found to be remarkably consistent showing, within uncertainties of the models, similar features including mantle temperatures. This is an important result as it shows that inverting EM sounding data directly for mantle thermal state is weakly dependent on the conductivity database employed to model bulk conductivity profiles.

For comparison Fig. 6 displays temperatures from petrological experiments on mineral phase transitions in the system $(Mg,Fe)_2SiO_4$. Ito and Takahashi (1989) found that the ol → wad and ring → fp + pv reactions (410- and 660-km) occurred at temperatures of ~1750 ± 100 K and ~1900 ± 150 K, respectively. In similar experiments Katsura et al. (2004) determined temperatures of 1760 ± 45 K and 1860 ± 50 K for these reactions, respectively. The inversions are in overall agreement with these experiments. Moreover, temperatures beneath the various localities follow surface tectonics to some extent in that the Archean craton (ASP) is generally found to be cold relative to a younger continental site (LZH).

8.2. Electrical conductivity structure

Conductivity structures obtained from inversion of long-period inductive response functions discussed in Section 2 are shown in Fig. 7, and their fits to observed data are shown in Figs. 8 and 9. Calculated inductive response functions from both databases fit the observations equally well with no real apparent differences. The non-monotonic increase in the real part of the observed C-responses at stations ASP and LZH is incompatible with the assumption of a 1-D conductivity structure (Weidelt, 1972), which likely reflects violation of assumed source structure (P_1^0) and/or possible contamination from the core in the period range in question. Note also that for stations LZH and ASP uncertainties increase at longer periods because of a shorter time span over which data were collected. These points were discussed further in Khan et al. (2011). We omit prior sampled conductivity models in Fig. 7 because conductivity is a secondary parameter and conditional on the primary parameters (mantle composition and temperature). As previously, we find that relative to the range of prior models the posterior range is much reduced. Data are not sensitive to crustal structure so that models are shown from the lithosphere on down.

The inversion-derived conductivity profiles beneath the four stations differ as observed earlier (Khan et al., 2011). As in the previous study, we note that TUC and LZH are more conductive in the upper mantle than are ASP and FUR, which conforms with the real part of the inductive response functions for periods ($\leq 10^6$ s), i.e., $\mathrm{Re}(C_{ASP,FUR}) > \mathrm{Re}(C_{LZH,TUC})$. This observation is also consistent with calculated temperature differences (Fig. 6). Strong conductivity increases associated with a thin melt layer are only observed beneath stations LZH (YK and KD) and TUC (YK only), while ASP and FUR for both databases have entirely melt-free results. This will be discussed further in the following section. Regional conductivity variations have also been reported in other 1-D mantle conductivity studies (e.g., Egbert and Booker, 1992; Lizzaralde et al., 1995; Neal et al., 2000;

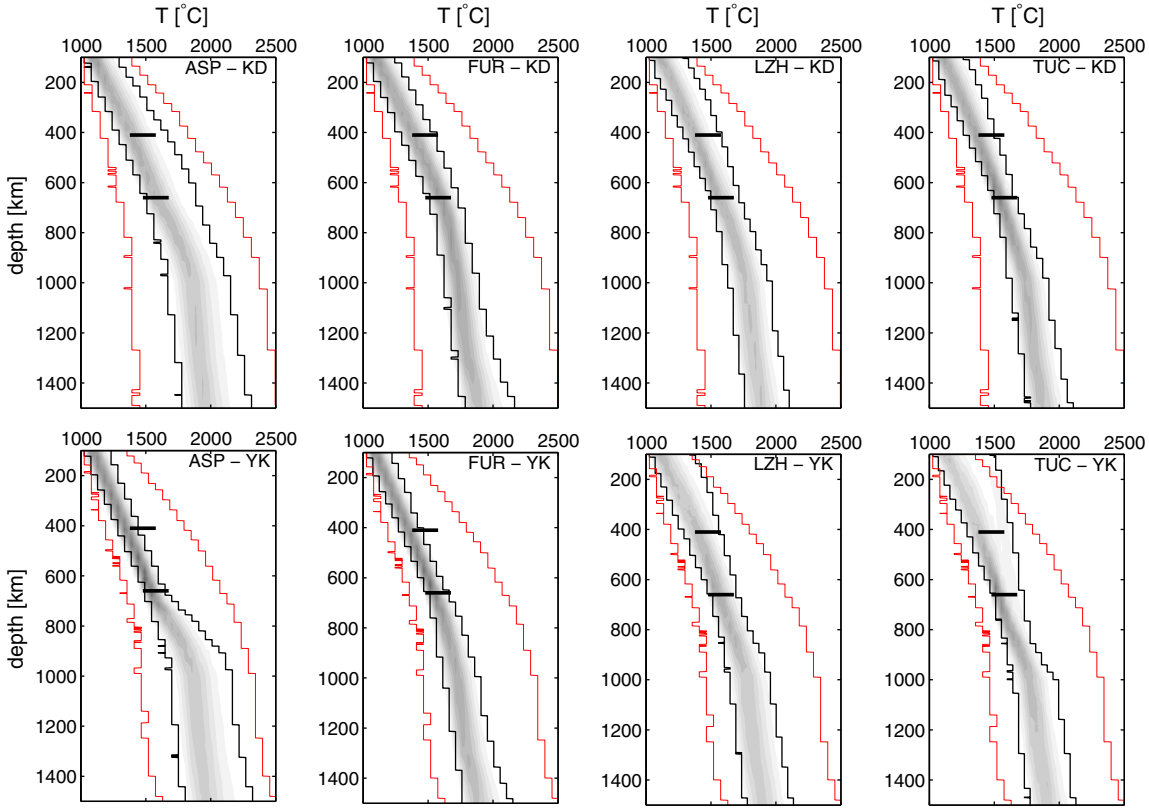

Fig. 6. Sampled prior and posterior geotherms beneath stations ASP, FUR, LZH, and TUC (observatories are defined in the main text) obtained using the KD (upper row) and YK (bottom row) databases, respectively. At each kilometer a histogram of the marginal probability distribution of sampled temperature was determined and by lining up these marginals, temperature as a function of depth is envisioned as contours directly relating their probability of occurrence. The contour lines define 20 equal-sized probability density intervals for the distributions, with black most probable and white least probable. Thin red and black lines indicate 99% prior and posterior credible intervals of sampled thermal models, respectively. Solid vertical bars indicate experimentally determined temperatures for the major mineral phase reactions at 410 and 660 km depth. See text for details.

Schultz and Larsen, 1987; Tarits et al., 2004) semiglobal (e.g., Fukao et al., 2004; Shimizu et al., 2010; Utada et al., 2009), and global studies (e.g., Kelbert et al., 2009; Semenov and Kuvshinov, 2011; Tarits and Mandea, 2010). Within the TZ and lower mantle, in particular, model discrepancies tend to narrow, although conductivities in the TZ beneath TUC and LZH appear slightly higher than ASP and FUR. In the lower mantle conductivity heterogeneities have been smoothed out, which is consistent with seismic tomography models (e.g., Kustowski et al., 2008; Panning and Romanowicz, 2006; Ritsema et al., 2011).

Further comparison of the models constructed from the two laboratory conductivity databases (Fig. 7) generally show an overall agreement, except for the highly conductive uppermost upper mantle, which is a distinct feature of the KD–TUC and KD–LZH profiles. This particular feature also appears at odds with the purely conductivity-derived models shown in Fig. 7, although the models overlap to a larger extent with those of Khan et al. (2011). It appears that this anomalously high conductivity is related to the strong increase in conductivity of hydrous ol and especially of hydrous opx for even small amounts of water that is an inherent feature of the KD database (Fig. 2). Another curious feature of the KD–TUC and KD–LZH profiles is the strong conductivity decrease that occurs just beneath ~300 km. Neither of the other two KD-based profiles (ASP and FUR) show such a marked behavior, hence the drops could be related to the above-mentioned high conductivities for depths (<300 km). Although low-conductivity bands are peculiar, they cannot be construed as a priori evidence against applying the KD database; they nonetheless suggest that the latter might be used with caution.

For comparison we also show the conductivity-derived subcontinental European conductivity model of Olsen (1999) and global model of Kuvshinov and Olsen (2006), the laboratory-based models of Khan et al. (2006) and Xu et al. (2000a), as well as those of Khan et al. (2011). Unlike purely geophysically-derived models, which are characterized by continuous conductivity increase through the mantle, the profiles presented here implicitly display discontinuities across major phase transitions and resemble earlier laboratory-based models. The general inability of EM fields to sense discontinuities results directly from their diffusive nature as evidenced in comparisons of conductivity models obtained here with those of, e.g., Khan et al. (2011).

Major differences between present and previous profiles are principally in the upper mantle and are mainly related to differing modeling aspects such as inversion for conductivity only, $d\sigma(r)/dr \geq 0$, and data sensitivity, among others. As discussed previously in Khan et al. (2011), although data are sensitive to upper mantle conductivity structure their main sensitivity lies in the TZ and uppermost lower mantle. We should mention that the models of Khan et al. (2006) and Xu et al. (2000a) also display a strong jump in electrical conductivity in the vicinity of the seismic 410-km discontinuity (ol → wad). This particular increase is not observed here because of using different mineral conductivity databases for major minerals, especially ol and wad. On the basis of measurements performed entirely on nominally anhydrous minerals, Xu et al. (2000a) measured a conductivity increase by at least an order of magnitude on going from ol to wad. In contrast, for a given constant upper mantle and TZ water content, the most recent experiments (YK) on hydrous equivalents hint at a smooth conductivity curve on crossing the 410-km discontinuity, while the anhydrous case suggests a decrease in conductivity (Fig. 2).

A consistent feature of all YK-based profiles is the jump in conductivity at ~520–540 km depth, which is related to the mineral

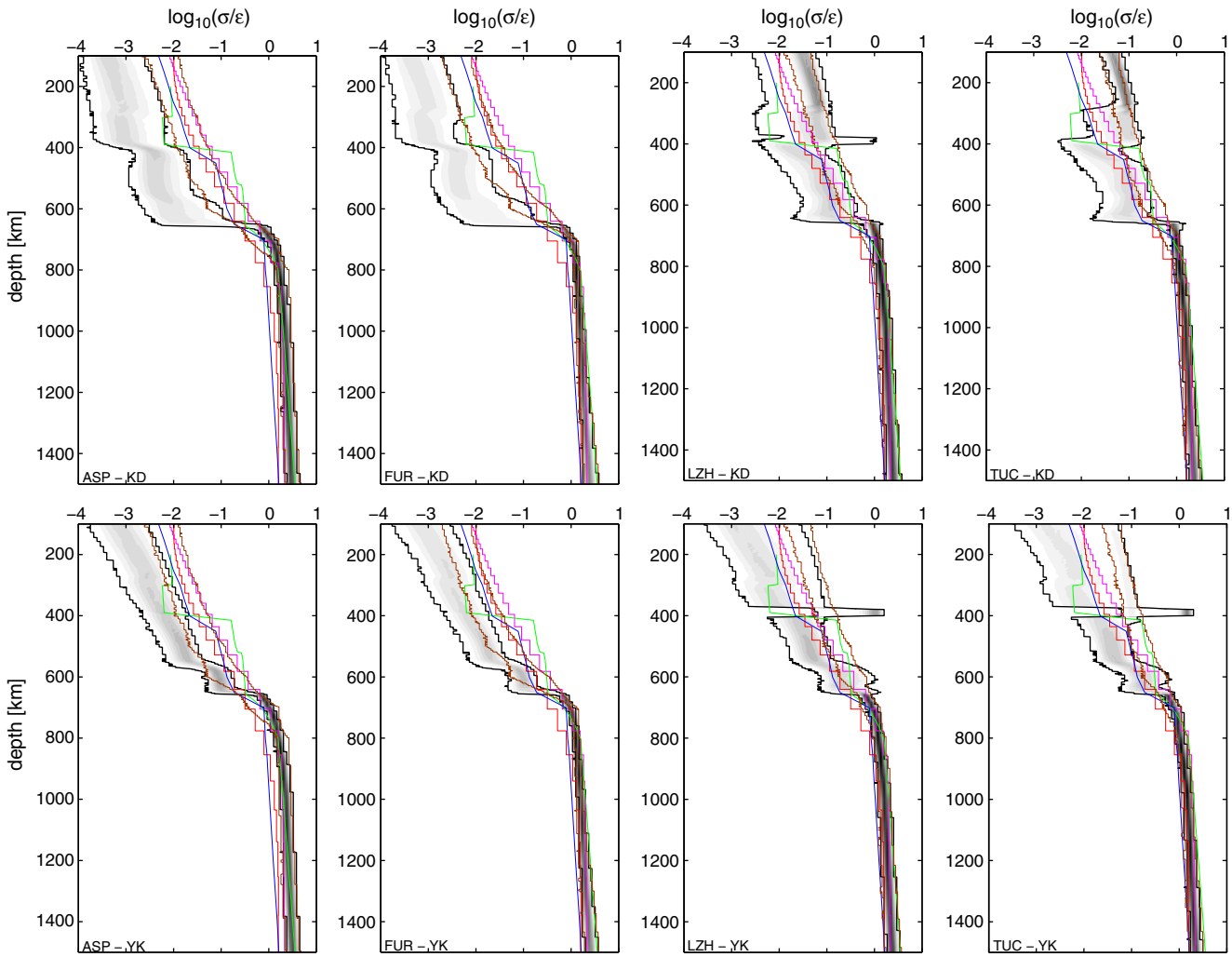

Fig. 7. Sampled posterior electrical conductivity profiles beneath stations ASP, FUR, LZH, and TUC (observatories are defined in the main text) obtained using the KD (upper row) and YK (bottom row) conductivity databases, respectively. At each kilometer a histogram of the marginal probability distribution of sampled conductivity was determined and by lining up these marginals, conductivity as a function of depth is envisioned as contours directly relating their probability of occurrence. The contour lines define 20 equal-sized probability density intervals for the distributions, with black most probable and white least probable. Thin black lines indicate 99% credible intervals of sampled conductivity models. For comparison some previous one-dimensional conductivity profiles are shown (thin lines): red — Olsen (1999); magenta — Kuvshinov and Olsen (2006); green — Xu et al. (2000a); blue — Khan et al. (2006); brown — upper and lower limits of the range of models (99% credible interval) from Khan et al. (2011). Note that the model of Khan et al. (2006) represents the mean profile and uncertainties (not shown) are generally of the order of ± 0.5 S/m. For the other profiles no uncertainty estimates exist. $\varepsilon = 1$ S/m.

transformation wad → ring. This feature is not produced in KD-based profiles. Because Eq. (8) lacks any conduction mechanism other than the single proton term, its ability to represent TZ conductivity is restricted.

Across the 660-km discontinuity (ring → fp + pv) conductivity increases abruptly by about one order of magnitude to 1 S/m for both databases. Further strong conductivity jumps are not observed in the lower mantle (to 1500 km depth), and conductivity increases only to a minor extent to ~2–7 S/m. As expected for the lower mantle, differences between conductivity profiles beneath all four stations are minimal because both databases employ the same measurements for pv and fp.

8.3. Mantle water content, hydration melting and high-conductivity upper-mantle melt layer

Compositional variations can also play an important role in determining conductivity structure (Figs. 2–4). We discuss only variations in upper mantle and TZ water content because data sensitivity to variations in major element composition is relatively minor given the somewhat narrow prior bounds on major element chemistry (Table 7). Apart from the indirect dependence of conductivity on composition through the influence of modal mineralogy, we only model a direct compositional dependence of conductivity through Eq. (6), which relates ringwoodite conductivity to Fe content as observed in experiments of Yoshino and Katsura (2009b).

Calculated mantle water content is shown in Fig. 10. Note that only water contents in olivine and wadsleyite are shown as C_w^{opx} and C_w^{gt} are fixed through the use of partition coefficients $\mathrm{D}_{\mathrm{H_2O}}^{\mathrm{opx/ol}}$ and $\mathrm{D}_{\mathrm{H_2O}}^{\mathrm{gt/ol}}$, respectively (Section 3.3). For both databases C_w^{ol} is for the most part constrained to be $\ll 0.05$ wt.% and by far the largest probability is centered on C_w^{ol} ~0–0.01 wt.%, Although minor variations occur for C_w^{ol}, both databases point to a relatively dry upper mantle beneath all four stations, with a somewhat larger variation in the case of the KD database. For orthopyroxene and garnet (KD database only, not shown) C_w^{opx}s in the ranges 0–0.1 wt.% (ASP and FUR) and 0–0.3 wt.% (LZH and TUC), respectively, are also observed, whereas C_w^{gt} is generally centered around 0 wt.%. These results largely agree with geochemical analyses of mantle rocks, for which water contents in the range from 0.0005 to 0.1 wt.% (e.g., Hirschmann et al., 2005)

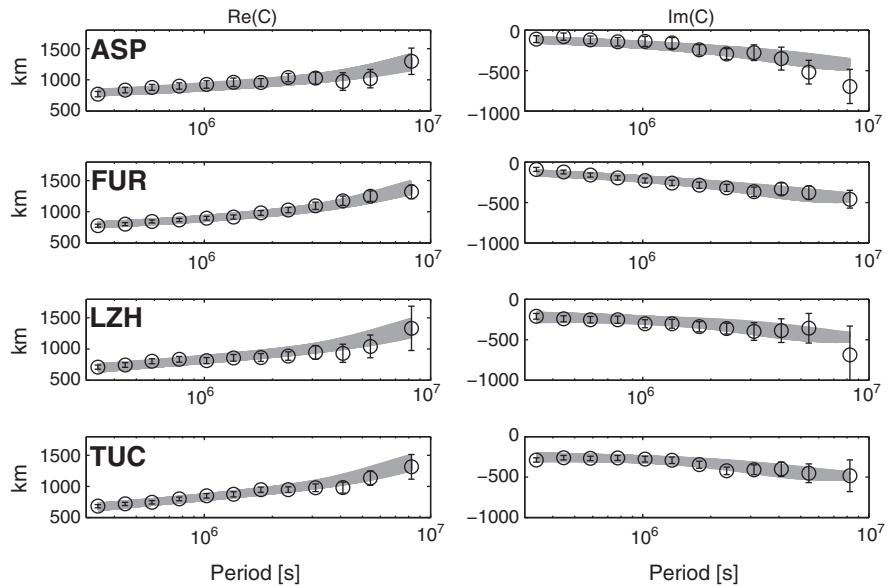

Fig. 8. Fit to inductive response functions (observed data — circles) and uncertainties (bars) from four geomagnetic observatories using the KD-based conductivity profiles in Fig. 7 (shaded bands — calculated data). Left and right columns depict real and imaginary parts of *C*-responses, respectively. For station details see main text and Table 1.

have been found. The petrologically determined water content, however, might not be representative of that in deeper rocks as samples derive from depths shallower than ~200 km. In the TZ discrepancies between the two laboratory databases become apparent. Overall, the KD database implies $C_w^{wad}<0.05$ wt.% with the bulk centered close to 0 wt.%. This somewhat contrasts with results obtained for the YK database where $C_w^{wad}>0.1$ wt.% is found to occur, in particular beneath LZH and TUC, although as in the case of KD, there is a high tendency for low values to be sampled.

Implications of these results for the presence of a highly conducting thin melt layer on top of the TZ are evident in Fig. 7. Only beneath stations LZH and TUC (both YK) are the water storage capacity of the upper mantle exceeded so that a thin melt layer appears with a relatively high probability. For the KD database only station LZH evidences a melt layer, although with such a low probability that upper mantle water storage capacity is not likely to be exceeded, hence formation of a hydrous silicate melt layer would be prevented. Toffelmier and Tyburczy (2007) using a different data set in their electromagnetic depth sounding study, also indicated the presence of a melt layer beneath station TUC. However, it should be mentioned that this conclusion is not robust inasmuch as their preferred model having a highly conductive (1 S/m) thin melt layer (5–30 thick) does not fit the EM data within uncertainties.

Using the YK database, Manthilake et al. (2009) concluded that a "dry" mantle model, i.e., a conductivity profile with $C_w=0$ wt.% throughout, agreed well with current semi-global conductivity profiles and thus that the concept of a globally hydrated mantle TZ needs not be invoked to explain mantle conductivity. On the other hand, on the basis of the

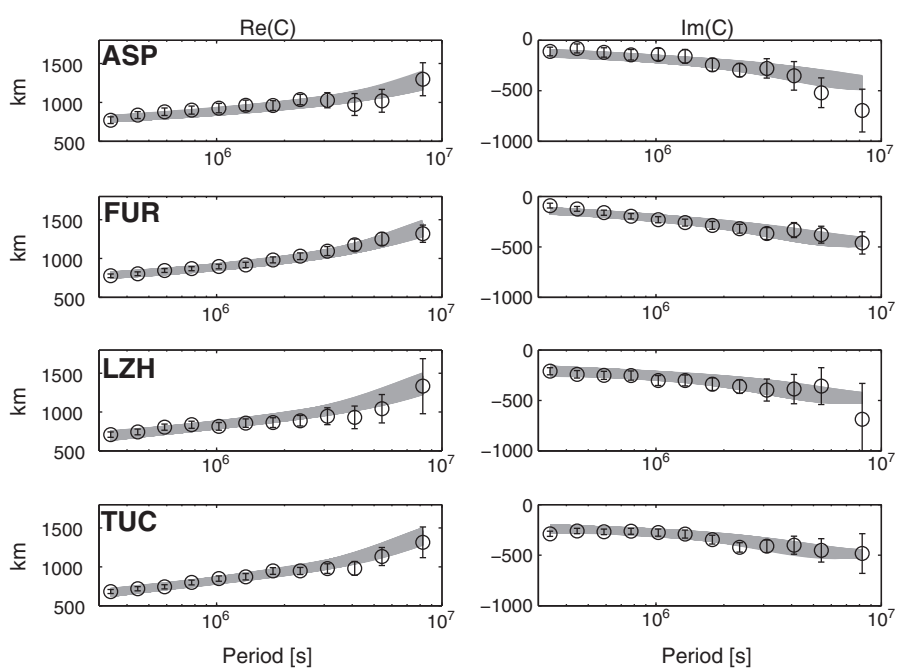

Fig. 9. Fit to inductive response functions (observed data — circles) and uncertainties (bars) from four geomagnetic observatories using the YK-based conductivity profiles in Fig. 7 (shaded bands — calculated data). Left and right columns depict real and imaginary parts of *C*-responses, respectively. For station details see main text and Table 1.

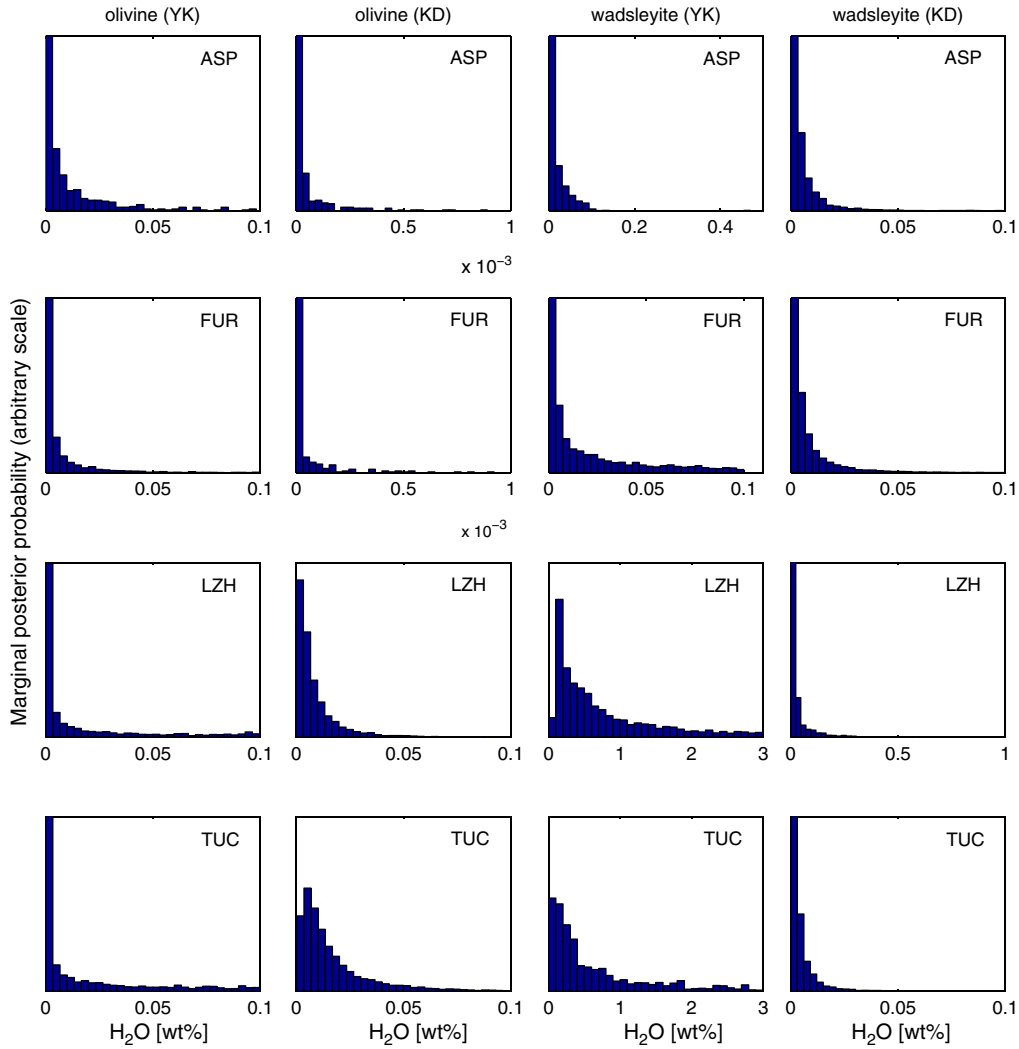

Fig. 10. Sampled water contents (C_w) in major upper mantle and transition zone minerals, olivine and wadsleyite, respectively. Sampled C_w values are displayed as marginal posterior probability distributions. KD (Karato, Dai and coworkers) and YK (Yoshino, Katsura and coworkers) refer to the two conductivity databases investigated. Observatories are defined in the main text. In the case of olivine ASP (KD) and FUR (KD) and wadsleyite, in general, only part of the sampled range of water contents is displayed for enhancement; full prior ranges encompass 0–0.1 wt.% for olivine and 0–3 wt.% for wadsleyite, respectively. See main text for details.

KD database Karato (2011) concluded that average water contents in the uppermost mantle and TZ are around 0.01 and 0.1 wt.%, respectively.

Thus, one observation of these treatments is that within the uncertainties of the two laboratory datasets a relatively "dry" uppermost mantle with <0.01 wt.% H_2O is consistent with both conductivity databases. Another observation is that according to the KD database the TZ should have a comparable water content of ~0.01 wt.% H_2O, implying absence of melt layer above the TZ as upper mantle water storage capacity is not exceeded. This contrasts with results from the YK database that show the TZ to be locally more hydrated with values reaching as much as 1–2 wt.%, thus enabling hydration melting and the presence of thin melt layers above the 410-km discontinuity. However, this result has to be considered in light of the relative sensitivity of YK- and KD-based conductivity profiles to changes in water content as discussed previously (see also Sections 6.1 and 6.3). This implies that the hypothesized water TZ filter of Bercovici and Karato (2003) occurs at most on a regional scale, in line with a similar conclusion drawn earlier by Toffelmier and Tyburczy (2007). Although tentative, a third observation is an indication of lateral variation: LZH–YK and TUC–YK appear to overlie more hydrated transition zones than do ASP and FUR, whereas LZH–KD and TUC–KD imply a more hydrated upper mantle than occurs beneath ASP and FUR.

Reasons for discrepancies between present results and earlier forward calculations (e.g., Karato, 2011; Manthilake et al., 2009) are most likely related to 1) the simplified nature of previous laboratory-based conductivity profiles (e.g., adiabatic geotherm, PREM-like pressure profile, mineralogy based on pyrolite composition) and 2) the largely qualitative comparison of these laboratory-based profiles with previous geophysically-derived conductivity profiles.

For completeness, we also considered the water storage capacity measurements of Tenner et al. (2011), who found values for olivine of 0.045±0.015 wt.% H2O at 400 km depth. Use of the lower bound, i.e., 0.03 wt.%, as a limiting value above which advected material from the TZ induces melting, resulted in no significant changes, in particular for the presence of high-conductivity melt layers in the deep upper mantle.

9. Summary and conclusion

This study uses a geophysical approach to estimating mantle composition (major element chemistry and water content) and thermal state by inverting a set of long-period electromagnetic sounding data beneath four geomagnetic stations at diverse tectonic settings. The connection between geophysical observables, physical rock properties (electrical conductivity), and thermo-chemistry is contained in the use of a self-consistent thermodynamic modeling scheme of mantle mineral phase equilibria that depend only on composition, temperature, and pressure. The great advantage of this approach is that it inserts

plausible geophysical/petrological knowledge of discontinuities that straightforward EM inversions would not be able to resolve even though they have to be present. Using inverse methods in the form of a stochastic-based algorithm, we sample these parameters to produce conductivity profiles fitting data within a range of uncertainties to obtain models of mantle conditions that simultaneously combine features of both laboratory and geophysical data.

The results indicate that the thermo-chemical state of the mantle can be reasonably well-retrieved given a set of high-quality inductive response functions and a consistent set of measurements of laboratory mineral conductivity and water partition coefficients. For conductivity data, we considered independent measurements from two experimental laboratories in order to minimize bias. Independent inversions using either database revealed similar features in mantle temperature structure beneath the four stations and agree well with experimentally-determined temperatures of major mantle phase transitions. Bulk conductivity profiles constructed from the thermo-chemical models were also found to broadly concur with geophysically-derived and previous laboratory-based conductivity profiles. The particular choice of partition coefficients between co-existing minerals appears to be of little importance. With regard to water content the results imply around 0–0.01 wt.% H_2O in the upper mantle, independent of the particular conductivity database employed. On the other hand, TZ water content seems to depend more on the particular choice of conductivity database. With the YK conductivity database much "wetter" (up to ~2 wt.% H_2O) minerals can fit the *C*-response data, resulting in localized thin melt layers above the TZ. Use of the KD equivalent, on the other hand, implies a relatively "dry" TZ and no melt layers.

Although this study has shown that it is indeed feasible to constrain mantle thermo-chemical state from inversion of long-period electromagnetic response functions, understanding how water shapes mantle processes nonetheless rests on key factors that will need to be considered in the future. Of main importance are 1) continued collection and refinement of the laboratory-based mineral conductivity database, 2) construction of high-quality inductive response functions of high coherency and small uncertainties, and not least 3) continued effort to extend the thermodynamic database employed in modeling mantle mineral phase equilibria. Point 2) includes extending the observed period range to improve sampling of both the upper mantle and the lower mantle and improving sensitivity throughout by decreasing data uncertainties, which presently limit inferences that can be drawn. Similarly, an improved experimental database for lower mantle conductivity, particularly of hydrous minerals, is needed.

In spite of any shortcomings of this analysis due to scarcity or absence of appropriate experimental data, it is our contention that a quantitative approach in which geophysical data are tested directly for fundamental parameters (composition and temperature) should be emphasized over approaches that rely on a plain comparison between geophysical models and forward models constructed from laboratory measurements.

Acknowledgments

We thank D. Dobson for critically reviewing the manuscript, which led to much improvement. An anonymous reviewer is also acknowledged for helpful input as is J. Connolly for informed discussions. This work was supported by Swiss National Science Foundation grant 200021-130411. Numerical computations were performed on the ETH cluster Brutus.

References

Ahrens, T.J., 1989. Water storage in the mantle. Nature 342, 122.
Aubaud, C., Hauri, E.H., Hirchmann, H.H., 2004. Hydrogen partition coefficients between nominally anhydrous minerals and basaltic melts. Geophys. Res. Lett. 31, L20611. doi:10.1029/2004GL021341.
Banks, R., 1969. Geomagnetic variations and the electrical conductivity of the upper mantle. Geophys. J. R. Astron. Soc. 17, 457.
Bell, D.R., Rossmann, G.R., Maldener, J., Endisch, D., Rauch, F., 2003. Hydroxide in olivine: a quantitative determination of the absolute amount and calibration of the IR spectrum. J. Geophys. Res. 108, 2105. doi:10.1029/2001JB000679.
Bercovici, D., Karato, S.-I., 2003. Whole-mantle convection and the transition-zone water filter. Nature 425, 39.
Berryman, J.G., 1995. Mixture theories for rock properties. In: Ahrens, T.J. (Ed.), American Geophysical Union Handbook of Physical Constants, 205. AGU, New York.
Bolfan-Casanova, N., 2005. Water in the Earth's mantle. Min. Mag. 69, 227.
Bolfan-Casanova, N., Keppler, H., Rubie, D.C., 2000. Partitioning of water between mantle phases in the system $MgO–SiO_2H_2O$ up to 24 GPa: implications for the distribution of water in the Earth's mantle. Earth Planet. Sci. Lett. 182, 209.
Bolfan-Casanova, N., McCammon, C.A., Mackwell, S.J., 2006. Water in transition zone and lower mantle minerals. In: Jacobsen, S.D., van der Lee, S. (Eds.), Earth's Deep Water Cycle. : Geophysical Monograph Series, 168. AGU. doi:10.1029/168GM06.
Brown, J.M., Shankland, T.J., 1981. Thermodynamic parameters in the Earth as determined from seismic profiles. Geophys. J. Roy. Astron. Soc. 66, 579.
Chen, J., Inoue, T., Yurimoto, H., Weidner, D.J., 2002. Effect of water on olivine–wadsleyite phase boundary in the $(Mg,Fe)_2SiO_4$ system. Geophys. Res. Lett. 29, 1875. doi:10.1029/2001GL014429.
Connolly, J.A.D., 2005. Computation of phase equilibria by linear programming: a tool for geodynamic modeling and an application to subduction zone decarbonation. Earth Planet. Sci. Lett. 236, 524.
Constable, S., 2006. SEO3: a new model of olivine electrical conductivity. Geophys. J. Int. 166, 435.
Dai, L., Karato, S.-I., 2009a. Electrical conductivity of orthopyroxene: implications for the water content of the asthenosphere. Proc. Jpn Acad. 85, 466.
Dai, L., Karato, S.-I., 2009b. Electrical conductivity of pyrope-rich garnet at high temperature and pressure. Phys. Earth Planet. Inter. 176. doi:10.1016/j.pepi.2009.04.002.
Dai, L., Karato, S.-I., 2009c. Electrical conductivity of wadsleyite at high temperatures and high pressure. Earth Planet. Sci. Lett.. doi:10.1016/j.epsl2009.08.012.
Dai, L., Li, H., Hu, H., Shan, S., 2008. Experimental study of grain boundary electrical conductivities of dry synthetic peridotites under high temperature, high-pressure, and different oxygen fugacity conditions. J. Geophys. Res. 113, B12211. doi:10.1029/2008JB005820.
Demouchy, S., Deloule, E., Frost, D.J., Keppler, H., 2005. Pressure and temperature-dependence of water solubility in iron-free wadsleyite. Am. Mineralog. 90, 1084.
Dobson, D.P., Brodholt, J.P., 2000a. The electrical conductivity and thermal profile of the Earth's mid-mantle. Geophys. Res. Lett. 27, 2325.
Dobson, D.P., Brodholt, J.P., 2000b. The electrical conductivity of the lower mantle phase magnesiowüstite at high temperatures and pressures. J. Geophys. Res. 105, 531.
Duba, A.G., Constable, S., 1993. The electrical conductivity of lherzolite. J. Geophys. Res. 98, 11885.
Duba, A.G., Shankland, T.J., 1982. Free carbon and electrical conductivity in the Earth's mantle. Geophys. Res. Lett. 9, 1271. doi:10.1029/GL009i011p01271.
Egbert, G., Booker, J.R., 1992. Very long period magnetotellurics at Tucson observatory: implications for mantle conductivity. J. Geophys. Res. 97, 15099.
Férot, A., Bolfan-Casanova, N., submitted for publication. Water storage capacity in olivine to 14 GPa and implications for the water content of the Earth's upper mantle. Earth Planet. Sci. Lett.
Fujii, I., Schultz, A., 2002. The 3D electromagnetic response of the Earth to ring current and auroral oval excitation. Geophys. J. Int. 151, 689.
Fukao, Y., Koyama, T., Obayashi, M., Utada, H., 2004. Trans-Pacific temperature field in the mantle transition region derived from seismic and electromagnetic tomography. Earth Planet. Sci. Lett. 217, 425.
Fullea, J., Muller, M.R., Jones, A.G., 2011. Electrical conductivity of continental lithospheric mantle from integrated geophysical and petrological modeling: application to the Kaapvaal Craton and Rehoboth Terrane, southern Africa. J. Geophys. Res. 116, B10202. doi:10.1029/2011JB008544.
Gaillard, F., 2004. Laboratory measurements of electrical conductivity of hydrous and dry silicic melts under pressure. Earth Planet. Sci. Lett. 218, 215. doi:10.1016/S0012-821X(03)00639-3.
Grant, K., Kohn, S., Brooker, R., 2004. Hydrogen partitioning between synthetic olivine, orthopyroxene and melt. Geochim. Cosmochim. Acta 68, A34.
Hashin, Z., Shtrikman, S., 1962. A variational approach to the theory of effective magnetic permeability of multiphase materials. J. Appl. Phys. 33, 3125.
Hauri, E.H., Gaetani, G.A., Green, T.H., 2004. Partitioning of H_2O between minerals and silicate melts. Geochim. Cosmochim. Acta 68, A33.
Hill, R., 1963. The elastic behaviour of crystalline aggregate. J. Mech. Phys. Solids 11, 357.
Hirschmann, M.M., 2006. Water, melting, and the deep Earth H_2O cycle. Ann. Rev. Earth Planet. Sci. 34, 629. doi:10.1146/annurev.earth.34.031405.125211.
Hirschmann, M.M., Aubaud, C., Withers, A.C., 2005. Storage capacity of H_2O in nominally anhydrous minerals in the upper mantle. Earth Planet. Sci. Lett. 236, 167. doi:10.1016/j.epsl.2005.04.022.
Hirschmann, M.M., Tenner, T., Aubaud, C., Withers, A.C., 2009. Dehydration melting of nominally anhydrous mantle: the primacy of partitioning. Phys. Earth Planet. Int. 176, 54. doi:10.1016/j.pepi.2009.04.001.
Hirth, G., Kohlstedt, D.L., 1996. Water in the oceanic upper mantle: implications for rheology, melt extraction and the evolution of the lithosphere. Earth Planet. Sci. Lett. 144, 93.
Hofmeister, A.M., 2004. Enhancement of radiative transfer in the upper mantle by OH- in minerals. Phys. Earth Planet. Inter. 146, 483.
Huang, X., Xu, Y., Karato, S.-I., 2005. Water content in the transition zone from electrical conductivity of wadsleyite and ringwoodite. Nature 434, 746.

Inoue, T., Yurimoto, H., Kudoh, Y., 1995. Hydrous modified spinel, Mg1.75SiH0.5O4, a new water reservoir in the mantle transition zone. J. Geophys. Res. 22, 117.
Irifune, T., 1994. Absence of an aluminous phase in the upper part of Earth's lower mantle. Nature 370, 131.
Ito, E., Takahashi, E., 1989. Postspinel transformations in the system Mg_2SiO_4–Fe_2SiO_4 and some geophysical implications. J. Geophys. Res. 94, 10637.
Jones, A.G., Evans, R.L., Eaton, D.W., 2009. Velocity–conductivity relationships for mantle mineral assemblages in Archean cratonic lithosphere based on a review of laboratory data and Hashin–Shtrikman extremal bounds. Lithos 109, 131. doi:10.1016/j.lithos.2008.10.014.
Karato, S.-I., 1990. The role of hydrogen in the electrical conductivity of the upper mantle. Nature 347, 272.
Karato, S.-I., 2006. Influence of hydrogen-related defects on the electrical conductivity and plastic deformation of mantle materials: a critical review. In: Jacobsen, S.D., van der Lee, S. (Eds.), Earth's Deep Water Cycle. AGU, Washington DC., p. 113.
Karato, S.-I., 2011. Water distribution across the mantle transition zone and its implications for global material circulation. Earth Planet. Sci. Lett. 301. doi:10.1016/j.epsl.2010.1.038.
Karato, S.-I., Dai, L., 2009. Comments on "Electrical conductivity of wadsleyite as a function of temperature and water content" by Manthilake et al. Phys. Earth Planet. Inter. doi:10.1016/j.pepi.2009.01.011.
Karato, S.-I., Jung, H., 2003. Effects of pressure on high-temperature dislocation creep in olivine polycrystals. Philos. Mag. A 83, 401.
Katsura, T., et al., 2004. Olivine–wadsleyite transition in the system $(Mg,Fe)_2SiO_4$. J. Geophys. Res. 109, B02209. doi:10.1029/2003JB002438.
Kelbert, A., Schultz, A., Egbert, G., 2009. Global electromagnetic induction constraints on transition-zone water content variations. Nature 460. doi:10.1038/nature08257.
Keppler, H., Bolfan-Casanova, N., 2006. Thermodynamics of water solubility and partitioning. Rev. Mineral. Geochem., Min. Soc. Am. 62, 193.
Khan, A., Connolly, J.A.D., Olsen, N., 2006. Constraining the composition and thermal state of the mantle beneath Europe from inversion of long-period electromagnetic sounding data. J. Geophys. Res. 111, B10102. doi:10.1029/2006JB004270.
Khan, A., Connolly, J.A.D., Maclennan, J., Mosegaard, K., 2007. Joint inversion of seismic and gravity data for lunar composition and thermal state. Geophys. J. Int. 168, 243. doi:10.1111/j.1365-246X.2006.03200.x.
Khan, A., Boschi, L., Connolly, J.A.D., 2009. On mantle chemical and thermal heterogeneities and anisotropy as mapped by inversion of global surface wave data. J. Geophys. Res. 114, B09305. doi:10.1029/2009JB006399.
Khan, A., Kuvshinov, A., Semenov, A., 2011. On the heterogeneous electrical conductivity structure of the Earth's mantle with implications for transition zone water content. J. Geophys. Res. 116, B01103. doi:10.1029/2010JB007458.
Koga, K., Hauri, E., Hirschmann, M.M., Bell, D., 2003. Hydrogen concentration analyses using SIMS and FTIR: comparison and calibration of for nominally anhydrous minerals. Geochem. Geophys. Geosyst. 4, 1019. doi:10.1029/2002GC000378.
Kohlstedt, D.L., Keppler, H., Rubie, D.C., 1996. Solubility of water in the α, β and γ phases of $(Mg,Fe)_2SiO_4$. Contrib. Mineral. Petrol. 123, 345.
Kustowski, B., Ekström, G., Dziewonski, A.M., 2008. Anisotropic shear-wave velocity structure of the Earth's mantle: a global model. J. Geophys. Res. 113, B06306. doi:10.1029/2007JB005169.
Kuvshinov, A., 2011. Deep electromagnetic studies from land, sea, and space: progress status in the past 10 years. Surv. Geophys.. doi:10.1007/s10712-011-9118-2
Kuvshinov, A., Olsen, N., 2006. A global model of mantle conductivity derived from 5 years of CHAMP, Ørsted, and SAC-C magnetic data. Geophys. Res. Lett. 33, L18301. doi:10.1029/2006GL027083.
Kuvshinov, A.V., Olsen, N., Avdeev, D.B., Pankratov, O.V., 2002. Electromagnetic induction in the oceans and the anomalous behaviour of coastal C-responses for periods up to 20 days. Geophys. Res. Lett. 29. doi:10.1029/2001GL014,409.
Landauer, R., 1952. The electrical resistance of binary metallic mixtures. J. Appl. Phys. 23, 779.
Ledo, J., Jones, A.G., 2005. Upper mantle temperature determined from combining mineral composition, electrical conductivity laboratory studies and magnetotelluric field observations: application to the Intermontane Belt, Northern Canadian Cordillera. Earth Planet. Sci. Lett. 236, 258.
Litasov, K.D., Ohtani, E., 2007. Effect of water on the phase relations in Earth's mantle and deep water cycle. In: Ohtani, E. (Ed.), Advances in High-pressure Mineralogy. Geological Soc. Amer., p. 115.
Litasov, K.D., Ohtani, E., Kagi, H., Jacobsen, S.D., 2007. Temperature dependence and mechanism of hydrogen incorporation in olivine at 12.5–14 GPa. Geophys. Res. Lett. 34 (L16314). doi:10.1029/2007GL030737.
Lizzaralde, D., Chave, A., Hirth, G., Schultz, A., 1995. Northeastern Pacific mantle conductivity profile from long-period magnetotelluric sounding using Hawaii to California submarine cable data. J. Geophys. Res. 100, 17837.
Lyubetskaya, T., Korenaga, J., 2007. Chemical composition of Earth's primitive mantle and its variance: 1. method and results. J. Geophys. Res. 112, B03211. doi:10.1029/2005JB004223.
Manthilake, M., Matsuzaki, T., Yoshino, T., Yamashita, S., Ito, E., Katsura, T., 2009. Electrical conductivity of wadsleyite as a function of temperature and water content. Phys. Earth Planet. Inter.. doi:10.1016/j.pepi.2008.06.001
Mao, Z., et al., 2008. Elasticity of hydrous wadsleyite to 12 GPa: implications for Earth's transition zone. Geophys. Res. Lett. 35, L21305. doi:10.1029/2008GL035618.
Maumus, J., Bagdassarov, N., Schmeling, H., 2005. Electrical conductivity and partial melting of mafic rocks under pressure. Geochim. Cosmochim. Acta 69, 4703. doi:10.1016/j.gca.2005.05.010.
Mei, S., Kohlstedt, D.L., 2000. Influence of water on plastic deformation of olivine aggregates, 2. dislocation creep regime. J. Geophys. Res. 105, 21471.
Mookherjee, M., Stixrude, L., Karki, B., 2008. Hydrous silicate melt at high pressure. Nature 452, 983. doi:10.1038/nature06918.
Mosegaard, K., Tarantola, A., 1995. Monte Carlo sampling of solutions to inverse problems. J. Geophys. Res. 100, 12431.
Mosenfelder, J., Deligne, N., Asimow, P., Rossmann, G.R., 2006. Hydrogen incorporation in olivine from 2 to 12 GPa. Am. Mineralog. 91, 285.
Neal, S.L., Mackie, R.L., Larsen, J.C., Schultz, A., 2000. Variations in the electrical conductivity of the upper mantle beneath North America and the Pacific Ocean. J. Geophys. Res. 105, 8229.
Ni, H., Keppler, H., Behrens, H., 2011. Electrical conductivity of hydrous basaltic melts: implications for partial melting in the upper mantle. Contrib. Mineral. Petrol. doi:10.1007/s00410-011-0617-4.
Ohtani, E., Litasov, K., Hosoya, T., Kubo, T., Kondo, T., 2004. Water transport into the deep mantle and formation of a hydrous transition zone. Phys. Earth Planet. Sci. 143. doi:10.1016/j.pepi.2003.09.015.
Olsen, N., 1999. Long-period (30 days–1 year) electromagnetic sounding and the electrical conductivity of the lower mantle beneath Europe. Geophys. J. Int. 138, 179.
Panning, M., Romanowicz, B., 2006. A three-dimensional radially anisotropic model of shear velocity in the whole mantle. Geophys. J. Int. 167, 361.
Park, S.K., Ducea, M.N., 2003. Can in situ measurements of mantle electrical conductivity be used to infer properties of partial melts? J. Geophys. Res. 108, 2270. doi:10.1029/2002JB001899.
Peslier, A., Woodland, A.B., Bell, D.R., Lazarov, M., 2010. Olivine water contents in the continental lithosphere and the longevity. Nature 467, 78. doi:10.1038/nature09317.
Poe, B., Romano, C., Nestola, F., Smyth, J.R., 2010. Electrical conductivity anisotropy of dry and hydrous olivine at 8 GPa. Phys. Earth Planet. Inter. 181, 103.
Pommier, A., Le Trong, E., 2011. "SIGMELTS": a web portal for electrical conductivity calculations in geosciences. Comput. Geosci. 37. doi:10.1016/j.cageo.2011.01.002.
Pommier, A., Gaillard, F., Malki, M., Pichavant, M., 2010. Reevaluation of the electrical conductivity of silicate melts. Am. Mineralog. 95, 284.
Rauch, M., Keppler, H., 2002. Water solubility in orthopyroxene. Contrib. Mineralog. Petrol. 78, 99.
Revenaugh, J., Sipkin, S.A., 1994. Seismic evidence for silicate melt atop the 410-km mantle discontinuity. Nature 369, 474.
Ringwood, A., 1975. Composition and Structure of the Earth's Mantle. McGraw-Hill, New York. 672 pp.
Ritsema, J., van Heijst, H.J., Deuss, A., Woodhouse, J.H., 2011. S40RTS: a degree-40 shear velocity model for the mantle from new Rayleigh wave dispersion, teleseismic traveltimes, and normal-mode splitting function measurements. Geophys. J. Int. 184. doi:10.1111/j.1365-246X.2010.04884.x.
Roberts, J.J., Tyburczy, J.A., 1993. Impedance spectroscopy of single and polycrystalline olivine: evidence for grain boundary transport. Phys. Chem. Miner. 20, 19. doi:10.1007/BF00202246.
Roberts, J.J., Tyburczy, J.A., 1999. Partial-melt electrical conductivity: influences of melt composition. J. Geophys. Res. 104, 7055.
Romano, C., Poe, B., Kreidie, N., McCammon, C., 2006. Electrical conductivities of pyrope-almandine garnets up to 19 GPa and 1700 °C. Am. Mineralog. 91, 1371.
Romano, C., Poe, B.T., Tyburczy, J., Nestola, F., 2009. Electrical conductivity of hydrous wadsleyite. Eur. J. Mineral. 21 (3), 615–622.
Schock, R.N., Duba, A.G., Shankland, T.J., 1989. Electrical conduction in olivine. J. Geophys. Res. 94, 5829.
Schultz, A., Larsen, J.C., 1987. On the electrical conductivity of the mid-mantle: I. calculation of equivalent scalar magnetotelluric response functions. Geophys. J. R. Astron. Soc. 88, 733.
Semenov, A., Kuvshinov, A., 2011. Global 3-D imaging of mantle conductivity based on inversion of ground-based C-responses: II. Results. Manuscript in preparation.
Shankland, T.J., Duba, A., 1990. Standard electrical conductivity of isotropic, homogeneous olivine in the temperature range 1200–1500 °C. Geophys. J. Int. 103, 25.
Shankland, T.J., Waff, H.S., 1977. Partial melting and electrical conductivities in the upper mantle. J. Geophys. Res. 82, 5409.
Shankland, T.J., O'Connell, R.J., Waff, H.S., 1981. Geophysical constraints on partial melt in the upper mantle. Rev. Geophys. Space Phys. 19, 394.
Shimizu, H., Utada, H., Baba, K., Koyama, T., Obayashi, M., Fukao, Y., 2010. Three-dimensional imaging of electrical conductivity in the mantle transition zone beneath the North Pacific Ocean by a semi-global induction study. Phys. Earth Planet. Inter. 183. doi:10.1016/j.pepi.2010.01.010.
Smyth, J.R., 1987. β-Mg_2SiO_4 a potential host for water in the mantle? Am. Mineralog. 72, 1051.
Smyth, J.R., Frost, D.J., 2002. The effect of water on the 410-km discontinuity: an experimental study. Geophys. Res. Lett. 29, 1485. doi:10.1029/2001GL014418.
Smyth, J.R., Frost, D.J., Nestola, F., Holl, C.M., Bromiley, G., 2006. Olivine hydration in the deep upper mantle: effects of temperature and silica activity. Geophys. Res. Lett. 33, L15301. doi:10.1029/2007GL030737.
Song, T.R.A., Helmberger, D.V., Grand, S.P., 2004. Low-velocity zone atop the 410-km seismic discontinuity in the northwestern United States. Nature 427, 530.
Stacey, F.D., Anderson, D.L., 2001. Electrical and thermal conductivities of Fe–Ni–Si alloy under core conditions. Phys. Earth Planet. Inter. 124, 153.
Stixrude, L., Lithgow-Bertelloni, C., 2005. Mineralogy and elasticity of the oceanic upper mantle: origin of the low-velocity zone. J. Geophys. Res. 110, B03204. doi:10.1029/2004JB002965.
Tarantola, A., Valette, B., 1982. Inverse problems=Quest for information. J. Geophys. 50, 159.
Tarits, P., Mandea, M., 2010. The heterogeneous electrical conductivity structure of the lower mantle. Phys. Earth Planet. Inter. 183. doi:10.1016/j.pepi.2010.08.002.
Tarits, P., Hautot, S., Perrier, F., 2004. Water in the mantle: results from electrical conductivity beneath French Alps. Geophys. Res. Lett. 31. doi:10.1029/2003GL019277.

Tauzin, B., Debayle, E., Wittlinger, G., 2010. Seismic evidence for a global low velocity layer in the Earth's upper mantle. Nat. Geosci. 3, 718. doi:10.1038/NGEO969.
ten Grotenhuis, S.M., Drury, M.R., Peach, C.J., Spiers, C.J., 2004. Electrical properties of fine-grained olivine: evidence for grain boundary transport. J. Geophys. Res. 109, B06203. doi:10.1029/2003JB002799.
Tenner, T.J., Hirschmann, M.M., Wither, A.C., Ardia, P., 2011. H_2O storage capacity of olivine and low-Ca pyroxene from 10 to 13 GPa: consequences for dehydration melting above the transition zone. Contrib. Mineral Petrol.. doi:10.1007/s00410-011-0675-7.
Toffelmier, D.A., Tyburczy, J.A., 2007. Electromagnetic detection of a 410-km-deep melt layer in the Southwestern United States. Nature 447. doi:10.1038/nature05922.
Tyburczy, J.A., Fisler, D.K., 1995. Electrical properties of minerals and melts. In: Ahrens, T.J. (Ed.), Mineral Physics and Crystallography: A Handbook of Physical Constants. AGU, Washington DC., p. 185.
Tyburczy, J.A., Waff, H.S., 1983. Electrical conductivity of molten basalt and andesite to 25 kilobars pressure: geophysical significance and implications for charge transport and melt structure. J. Geophys. Res. 88, 2413. doi:10.1029/JB088iB03p02413.
Utada, H., Koyama, T., Obayashi, M., Fukao, Y., 2009. A joint interpretation of electromagnetic and seismic tomography models suggests the mantle transition zone below Europe is dry. Earth Planet. Sci. Lett.. doi:10.1016/j.epsl.2009.02.027
Vacher, P., Verhoeven, O., 2007. Modelling the electrical conductivity of iron-rich minerals for planetary applications. Planet. Space Sci. 55, 455. doi:10.1016/j.pss.2006.10.003.
Verhoeven, O., et al., 2009. Constraints on thermal state and composition of the Earth's lower mantle from electromagnetic impedances and seismic data. J. Geophys. Res. 114, B03302. doi:10.1029/2008JB005678.
Waff, H.S., 1974. Theoretical considerations of electrical conductivity in a partially molten mantle and implications for geothermobarometry. J. Geophys. Res. 79, 4003.
Wang, D., Mookherjee, M., Xu, Y., Karato, S.-I., 2006. The effect of water on the electrical conductivity in olivine. Nature 443, 977.
Watson, H.C., Roberts, J.J., Tyburczy, J.A., 2010. Effect of conductive impurities on electrical conductivity in polycrystalline olivine. Geophys. Res. Lett. 37, L02302. doi:10.1029/2009GL041566.
Watt, J.P., Davies, G.F., O'Connell, R.J., 1976. The elastic properties of composite materials. Rev. Geophys. Space Phys. 14, 541.
Weidelt, P., 1972. The inverse problem of geomagnetic induction. Z. Geophys. 38 (257), 1972.
Wood, B.J., 1995. The effect of H_2O on the 410-kilometer seismic discontinuity. Science 268, 71.
Wu, X., et al., 2010. Electrical conductivity measurements of periclase under high pressure and high temperature. Physica B 405. doi:10.1016/j.physb.2009.08.036.
Xu, Y., Shankland, T.J., 1999. Electrical conductivity of orthopyroxene and its high pressure phases. Geophys. Res. Lett. 26, 2645.
Xu, Y., McCammon, C., Poe, B.T., 1998. The effect of alumina on the electrical conductivity of silicate perovskite. Science 282, 922.
Xu, Y., Shankland, T.J., Poe, B.T., 2000a. Laboratory-based electrical conductivity in the Earth's mantle. J. Geophys. Res. 108, 2314.
Xu, Y., Shankland, T.J., Duba, A.G., 2000b. Pressure effect on electrical conductivity of mantle olivine. Phys. Earth Planet. Inter. 118, 149.
Xu, W., Lithgow-Bertelloni, C., Stixrude, L., Ritsema, J., 2008. The effect of bulk composition and temperature on mantle seismic structure. Earth Planet. Sci. Lett. doi:10.1016/j.epsl.2008.08.012.
Yoshino, T., 2010. Laboratory electrical conductivity measurements of mantle minerals. Surv. Geophys. 31, 163.
Yoshino, T., Katsura, T., 2009a. Reply to comments on "Electrical conductivity of wadsleyite as a function of temperature and water content" by Manthilake et al. Phys. Earth Planet. Inter.. doi:10.1016/j.pepi.2009.01.012
Yoshino, T., Katsura, T., 2009b. Effect of iron content on electrical conductivity of ringwoodite, with implications for electrical structure in the transition zone. Phys. Earth Planet. Inter.. doi:10.1016/j.pepi.2008.09.015
Yoshino, T., Matsuzaki, T., Yamashita, S., Katsura, T., 2006. Hydrous olivine unable to account for conductivity anomaly at the top of the asthenosphere. Nature 443. doi:10.1038/nautre05223.
Yoshino, T., Nishi, M., Matsuzaki, T., Yamazaki, D., Katsura, T., 2008a. Electrical conductivity of majorite garnet and its implications for electrical structure in the mantle transition zone. Phys. Earth Planet. Inter.. doi:10.1016/j.pepi.2008.04.009.
Yoshino, T., Manthilake, G., Matsuzaki, T., Katsura, T., 2008b. Dry mantle transition zone inferred from the conductivity of wadsleyite and ringwoodite. Nature 451. doi:10.1038/nautre06427.
Yoshino, T., Matsuzaki, T., Shatskiy, A., Katsura, T., 2009. The effect of water on the electrical conductivity of olivine aggregates and its implications for the electrical structure of the upper mantle. Earth Planet. Sci. Lett.. doi:10.1016/j.epsl.2009.09.032.
Yoshino, T., Laumonier, M., McIsaac, E., Katsura, T., 2010. Electrical conductivity of basaltic and carbonatite melt-bearing peridotites at high pressures: implications for melt distribution and melt fraction in the upper mantle. Earth Planet. Sci. Lett. doi:10.1016/j.epsl.2010.04.050.